Signal processing on spherical manifolds

Jason McEwen

http://www.jasonmcewen.org/

Department of Physics and Astronomy
University College London (UCL)

Australian National University (ANU) :: March 2013

Observations on spherical manifolds
Earth

Credit: NASA

Observations on spherical manifolds

Interior of the Earth

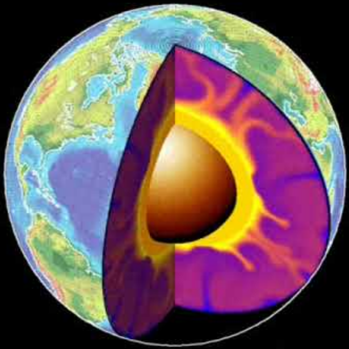

Credit: http://maps.unomaha.edu/

Observations on spherical manifolds

Diffusion magnetic resonance imaging

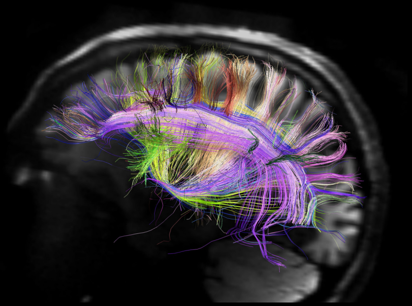

Credit: http://neuroimages.tumblr.com/

Observations on spherical manifolds
Computer graphics

Credit: http://www.pauldebevec.com

Observations on spherical manifolds
Computer graphics

Observations on spherical manifolds
Cosmology

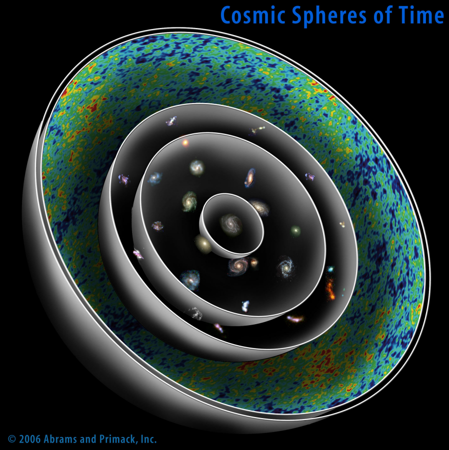

Outline

Outline

Cosmological concordance model

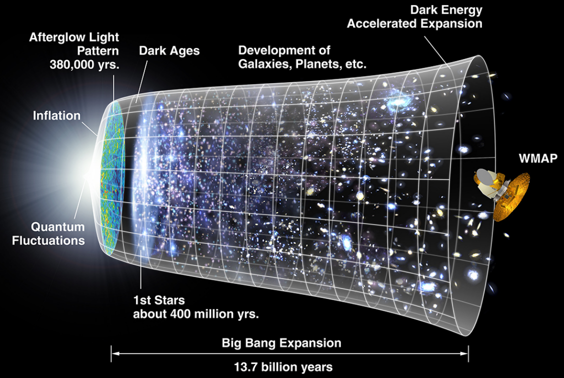

Credit: WMAP Science Team

Cosmic microwave background (CMB)

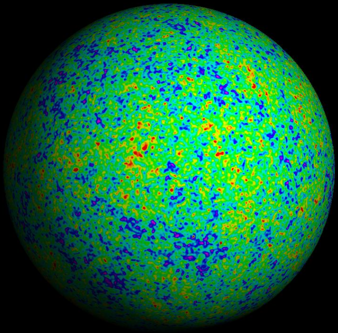

Credit: WMAP

Observations of the cosmic microwave background (CMB)

- Full-sky observations of the CMB ongoing.

(a) COBE (launched 1989)

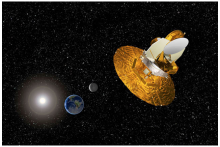

(b) WMAP (launched 2001)

(c) Planck (launched 2009)

- Each new experiment provides dramatic improvement in precision and resolution of observations.

(cobe 2 wmap movie)

(planck movie)

(d) COBE to WMAP [Credit: WMAP Science Team]

(e) Planck observing strategy [Credit: Planck Collaboration]

Cosmic microwave background (CMB)

- Temperature of early Universe sufficiently hot that photons had enough energy to ionise hydrogen.
- Compton scattering happened frequently $\Rightarrow$ mean free path of photons extremely small.
- Universe consisted of an opaque photon-baryon fluid.
- As Universe expanded it cooled, until majority of photons no longer had sufficient energy to ionise hydrogen.
- Photons decoupled from baryons and the Universe became essentially transparent to radiation.
- *Recombination* occurred when temperature of Universe dropped to 3000K ($\sim$400,000 years after the Big Bang).
- Photons then free to propagate largely unhindered and observed today on celestial sphere as CMB radiation.
- CMB is highly uniform over the celestial sphere, however it contains small fluctuations at a relative level of 10^{-5} due to acoustic oscillations in the early Universe.
- CMB observed on spherical manifold, hence the geometry of the sphere must be taken into account in any analysis.

Cosmic microwave background (CMB)

- Temperature of early Universe sufficiently hot that photons had enough energy to ionise hydrogen.
- Compton scattering happened frequently $\Rightarrow$ mean free path of photons extremely small.
- Universe consisted of an opaque photon-baryon fluid.
- As Universe expanded it cooled, until majority of photons no longer had sufficient energy to ionise hydrogen.
- Photons decoupled from baryons and the Universe became essentially transparent to radiation.
- *Recombination* occurred when temperature of Universe dropped to 3000K ($\sim$400,000 years after the Big Bang).
- Photons then free to propagate largely unhindered and observed today on celestial sphere as CMB radiation.
- CMB is highly uniform over the celestial sphere, however it contains small fluctuations at a relative level of 10^{-5} due to acoustic oscillations in the early Universe.
- CMB observed on spherical manifold, hence the geometry of the sphere must be taken into account in any analysis.

Cosmic microwave background (CMB)

- Temperature of early Universe sufficiently hot that photons had enough energy to ionise hydrogen.
- Compton scattering happened frequently $\Rightarrow$ mean free path of photons extremely small.
- Universe consisted of an opaque photon-baryon fluid.
- As Universe expanded it cooled, until majority of photons no longer had sufficient energy to ionise hydrogen.
- Photons decoupled from baryons and the Universe became essentially transparent to radiation.
- *Recombination* occurred when temperature of Universe dropped to 3000K ($\sim$400,000 years after the Big Bang).

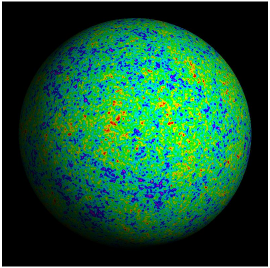

Credit: Max Tegmark

- Photons then free to propagate largely unhindered and observed today on celestial sphere as CMB radiation.
- CMB is highly uniform over the celestial sphere, however it contains small fluctuations at a relative level of 10^{-5} due to acoustic oscillations in the early Universe.
- CMB observed on spherical manifold, hence the geometry of the sphere must be taken into account in any analysis.

Cosmic microwave background (CMB)

- Quantum fluctuations in the early Universe blown to macroscopic scales by inflation, establishing acoustic oscillations in primordial plasma of the very early Universe.
- Provide the seeds of structure formation in our Universe.
- Cosmological concordance model explains the power spectrum of these oscillations to very high precision.
- Although a general cosmological concordance model is now established, many details remain unclear. Study of more exotic cosmological models now important.

Cosmic microwave background (CMB)

- Quantum fluctuations in the early Universe blown to macroscopic scales by inflation, establishing acoustic oscillations in primordial plasma of the very early Universe.
- Provide the seeds of structure formation in our Universe.
- Cosmological concordance model explains the power spectrum of these oscillations to very high precision.

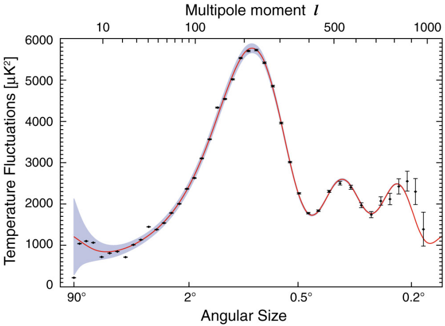

Credit: WMAP Science Team

- Although a general cosmological concordance model is now established, many details remain unclear. Study of more exotic cosmological models now important.

Cosmic microwave background (CMB)

- Quantum fluctuations in the early Universe blown to macroscopic scales by inflation, establishing acoustic oscillations in primordial plasma of the very early Universe.
- Provide the seeds of structure formation in our Universe.
- Cosmological concordance model explains the power spectrum of these oscillations to very high precision.

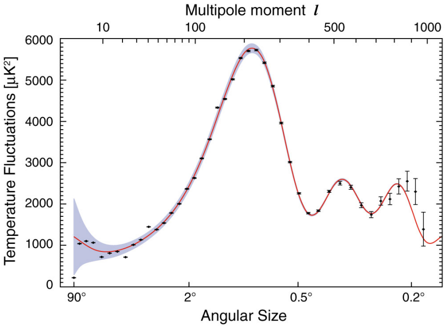

Credit: WMAP Science Team

- Although a general cosmological concordance model is now established, many details remain unclear. Study of more exotic cosmological models now important.

Galaxy surveys

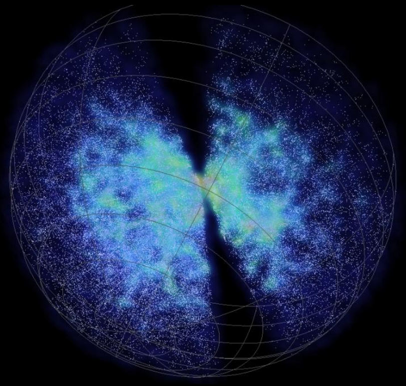

Credit: SDSS

A new era of observational cosmology

- We are entering a new era of observational cosmology:
  - Planck will provide full-sky observations of the cosmic microwave background (CMB) at unprecedented resolution, sensitivity and frequency coverage.
  - The Dark Energy Survey (DES) will survey of an order of magnitude more galaxies than the previous state-of-the-art.
  - The Euclid mission will survey more than a billion galaxies over more than one third of the sky, with unprecedented precision.
  - The Square Kilometre Array (SKA) will have a sensitivity 50x that of previous radio telescopes.

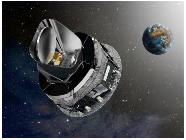

(a) Planck

(b) DES

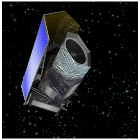

(c) Euclid

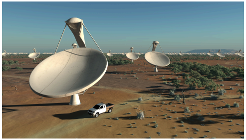

(d) SKA

- BUT... in order to develop a deeper understanding of cosmology, new instruments must be complemented with novel scientific analyses.

A new era of observational cosmology

- We are entering a new era of observational cosmology:
  - Planck will provide full-sky observations of the cosmic microwave background (CMB) at unprecedented resolution, sensitivity and frequency coverage.
  - The Dark Energy Survey (DES) will survey of an order of magnitude more galaxies than the previous state-of-the-art.
  - The Euclid mission will survey more than a billion galaxies over more than one third of the sky, with unprecedented precision.
  - The Square Kilometre Array (SKA) will have a sensitivity 50x that of previous radio telescopes.

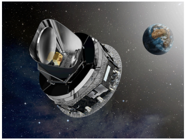
(a) Planck


(b) DES

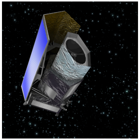
(c) Euclid

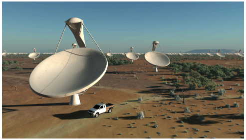
(d) SKA

- BUT... in order to develop a deeper understanding of cosmology, new instruments must be complemented with novel scientific analyses.

Outline

Spherical harmonic transform

- The spherical harmonics are the eigenfunctions of the Laplacian on the sphere: $\Delta_{\mathbb{S}^2} Y_{\ell m} = -\ell(\ell+1) Y_{\ell m}$.

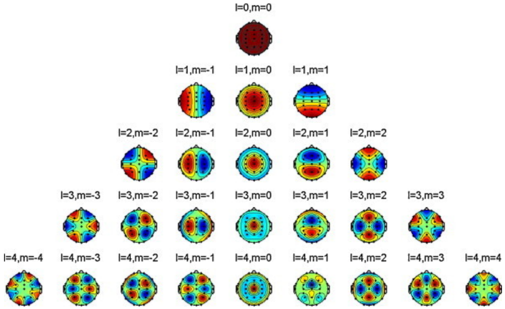

Figure: Spherical harmonic functions.

Spherical harmonic transform

- A function on the sphere $f \in \mathrm{L}^2(\mathbb{S}^2)$ may be represented by its spherical harmonic expansion:

$$f(\theta, \varphi) = \sum_{\ell=0}^{\infty} \sum_{m=-\ell}^{\ell} f_{\ell m} \, Y_{\ell m}(\theta, \varphi) \; .$$

  where the spherical harmonic coefficients are given by:

$$f_{\ell m} = \langle f, \, Y_{\ell m} \rangle = \int_{\mathbb{S}^2} \mathrm{d}\Omega(\theta, \varphi) \, f(\theta, \varphi) \, Y_{\ell m}^*(\theta, \varphi) \; .$$

- Consider signals on the sphere band-limited at L, that is signals such that $\boxed{f_{\ell m} = 0, \; \forall \ell \geq L}$.

- For a band-limited signal, can we compute $f_{\ell m}$ exactly?

  $\rightarrow$ Sampling theorems on the sphere

Driscoll & Healy (DH) sampling theorem

- Canonical sampling theorem on the sphere derived by Driscoll & Healy (1994).

$\Rightarrow$ $N_{\rm DH} = (2L-1)2L + 1 \sim 4L^2$ samples on the sphere.

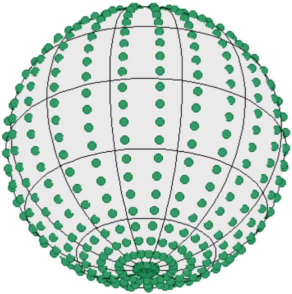

Figure: Sample positions of the DH sampling theorem.

McEwen & Wiaux (MW) sampling theorem

- A new sampling theorem on the sphere (McEwen & Wiaux 2011).

  $\Rightarrow$ $N_{\mathrm{MW}} = (L-1)(2L-1)+1 \sim 2L^2$ samples on the sphere.

- Reduced the Nyquist rate on the sphere by a factor of two.

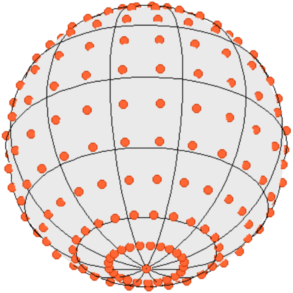

Figure: Sample positions of the MW sampling theorem.

McEwen & Wiaux (MW) sampling theorem

- New sampling theorem follows by associating the sphere with the torus through a periodic extension.
- Similar in flavour to making a periodic extension in θ of a function f on the sphere.

(a) Function on sphere (b) Even function on torus (c) Odd function on torus

Figure: Associating functions on the sphere and torus

McEwen & Wiaux (MW) sampling theorem

- By a factoring of rotations, a reordering of summations and a separation of variables, the inverse transform of ${}_sf$ may be written:

Inverse spherical harmonic transform

$$ {}_sf(\theta,\varphi) = \sum_{m=-(L-1)}^{L-1} {}_sF_m(\theta)\, e^{im\varphi} $$

$$ {}_sF_m(\theta) = \sum_{m'=-(L-1)}^{L-1} {}_sF_{mm'}\, e^{im'\theta} $$

$$ {}_sF_{mm'} = (-1)^s\, i^{-(m+s)} \sum_{\ell=0}^{L-1} \sqrt{\frac{2\ell+1}{4\pi}}\, \Delta^{\ell}_{m'm}\, \Delta^{\ell}_{m',-s}\, {}_sf_{\ell m} $$

where $\Delta^{\ell}_{mn} \equiv d^{\ell}_{mn}(\pi/2)$ are the reduced Wigner functions evaluated at $\pi/2$.

McEwen & Wiaux (MW) sampling theorem

- By a factoring of rotations, a reordering of summations and a separation of variables, the forward transform of ${}_sf$ may be written:

Forward spherical harmonic transform

$$ {}_sf_{\ell m} = (-1)^s \, \mathrm{i}^{m+s} \sqrt{\frac{2\ell+1}{4\pi}} \sum_{m'=-(L-1)}^{L-1} \Delta^{\ell}_{m'm} \, \Delta^{\ell}_{m',-s} \, {}_sG_{mm'} $$

$$ {}_sG_{mm'} = \int_0^{\pi} \mathrm{d}\theta \, \sin\theta \, {}_sG_m(\theta) \, \mathrm{e}^{-\mathrm{i}m'\theta} $$

$$ {}_sG_m(\theta) = \int_0^{2\pi} \mathrm{d}\varphi \, {}_sf(\theta,\varphi) \, \mathrm{e}^{-\mathrm{i}m\varphi} $$

Comparison
Numerical accuracy

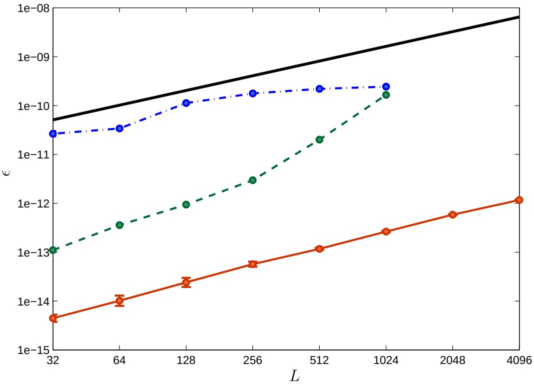

Figure: Numerical accuracy (MW=red; DH=green; GL=blue)

Comparison
Computation time

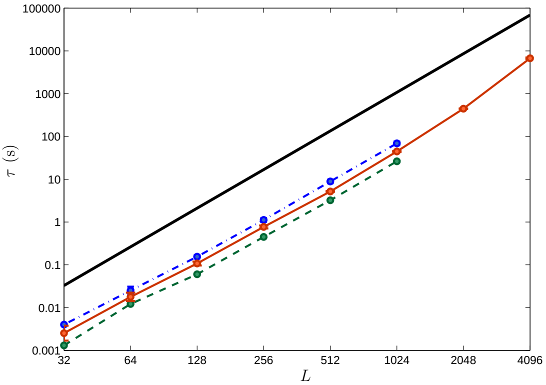

Figure: Computation time (MW=red; DH=green; GL=blue)

Comparison

	DH Divide-and-conquer	DH Semi-naive	MW
Pixelisation scheme	equiangular	equiangular	equiangular
Asymptotic complexity	$\mathcal{O}(L^{5/2} \log_2^{1/2} L)$	$\mathcal{O}(L^3)$	$\mathcal{O}(L^3)$
Precomputation	Y	N	N
Stability	N	Y	Y
Flexibility of Wigner recursion	N	N	Y
Spin functions	N	N	Y
Number of samples	$\mathbf{4L^2}$	$\mathbf{4L^2}$	$\mathbf{2L^2}$

Sampling theorem on the ball

- Fourier-Bessel functions are the canonical orthogonal basis on the sphere $\rightarrow$ but do not admit a sampling theorem.
- Developed a new Fourier-Laguerre transform and the first sampling theorem on the ball (Leistedt & McEwen 2012).

Sampling theorem on the ball

- Fourier-Bessel functions are the canonical orthogonal basis on the sphere $\rightarrow$ but do not admit a sampling theorem.
- Developed a new Fourier-Laguerre transform and the first sampling theorem on the ball (Leistedt & McEwen 2012).

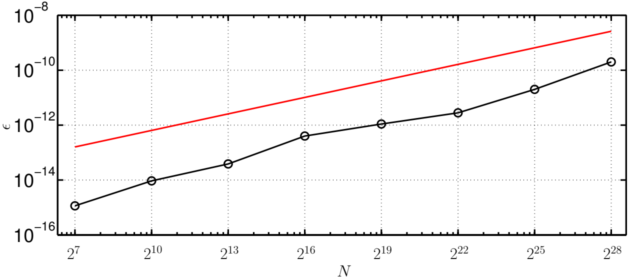

Figure: Numerical accuracy of Fourier-Laguerre transform

Sampling theorem on the ball

- Fourier-Bessel functions are the canonical orthogonal basis on the sphere → but do not admit a sampling theorem.
- Developed a new Fourier-Laguerre transform and the first sampling theorem on the ball (Leistedt & McEwen 2012).

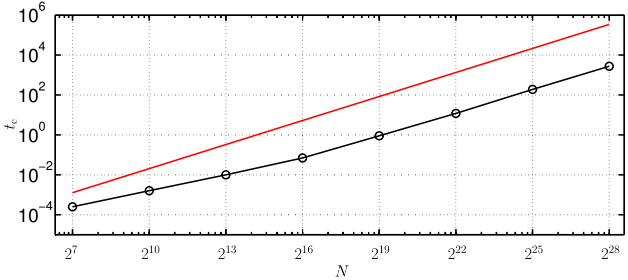

Figure: Computation time of Fourier-Laguerre transform

Codes to compute harmonic transforms

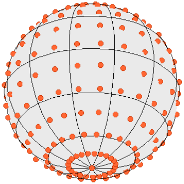

SSHT code: Spin spherical harmonic transforms
A novel sampling theorem on the sphere
McEwen & Wiaux (2011)

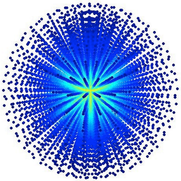

FLAG code: Fourier-Laguerre transforms
Exact wavelets on the ball
Leistedt & McEwen (2012)

All codes available from: `http://www.jasonmcewen.org/`

Outline

Wavelet transform in Euclidean space

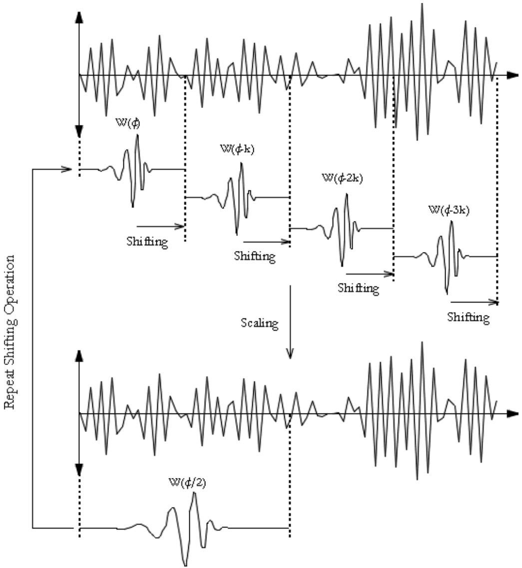

Figure: Wavelet scaling and shifting (Credit: `http://www.wavelet.org/tutorial/`)

Continuous wavelets on the sphere

- First natural wavelet construction on the sphere was derived in the seminal work of Antoine and Vandergheynst (1998) (reintroduced by Wiaux 2005).
- Construct wavelet atoms from affine transformations (dilation, translation) on the sphere of a mother wavelet.
- The natural extension of translations to the sphere are rotations. Rotation of a function f on the sphere is defined by

$$[\mathcal{R}(\rho)f](\omega) = f(\rho^{-1}\omega), \quad \omega = (\theta, \varphi) \in \mathbb{S}^2, \quad \rho = (\alpha, \beta, \gamma) \in \mathrm{SO}(3) .$$

- How define dilation on the sphere?
- The spherical dilation operator is defined through the conjugation of the Euclidean dilation and stereographic projection Π:

$$\mathcal{D}(a) \equiv \Pi^{-1}\, d(a)\, \Pi .$$

Continuous wavelets on the sphere

- First natural wavelet construction on the sphere was derived in the seminal work of Antoine and Vandergheynst (1998) (reintroduced by Wiaux 2005).
- Construct wavelet atoms from affine transformations (dilation, translation) on the sphere of a mother wavelet.
- The natural extension of translations to the sphere are rotations. Rotation of a function f on the sphere is defined by

$$[\mathcal{R}(\rho)f](\omega) = f(\rho^{-1}\omega), \quad \omega = (\theta, \varphi) \in \mathbb{S}^2, \quad \rho = (\alpha, \beta, \gamma) \in \mathrm{SO}(3) \ .$$

- How define dilation on the sphere?
- The spherical dilation operator is defined through the conjugation of the Euclidean dilation and stereographic projection Π:

$$\mathcal{D}(a) \equiv \Pi^{-1}\, d(a)\, \Pi \ .$$

Continuous wavelets on the sphere

- First natural wavelet construction on the sphere was derived in the seminal work of Antoine and Vandergheynst (1998) (reintroduced by Wiaux 2005).
- Construct wavelet atoms from affine transformations (dilation, translation) on the sphere of a mother wavelet.
- The natural extension of translations to the sphere are rotations. Rotation of a function f on the sphere is defined by

$$[\mathcal{R}(\rho)f](\omega) = f(\rho^{-1}\omega), \quad \omega = (\theta, \varphi) \in \mathbb{S}^2, \quad \rho = (\alpha, \beta, \gamma) \in \mathrm{SO}(3) \ .$$

- How define dilation on the sphere?
- The spherical dilation operator is defined through the conjugation of the Euclidean dilation and stereographic projection Π:

$$\mathcal{D}(a) \equiv \Pi^{-1}\, d(a)\, \Pi \ .$$

Continuous wavelets on the sphere

- First natural wavelet construction on the sphere was derived in the seminal work of Antoine and Vandergheynst (1998) (reintroduced by Wiaux 2005).
- Construct wavelet atoms from affine transformations (dilation, translation) on the sphere of a mother wavelet.
- The natural extension of translations to the sphere are rotations. Rotation of a function f on the sphere is defined by

$$[\mathcal{R}(\rho)f](\omega) = f(\rho^{-1}\omega), \quad \omega = (\theta, \varphi) \in \mathbb{S}^2, \quad \rho = (\alpha, \beta, \gamma) \in \mathrm{SO}(3) \ .$$

- How define dilation on the sphere?
- The spherical dilation operator is defined through the conjugation of the Euclidean dilation and stereographic projection Π:

$$\mathcal{D}(a) \equiv \Pi^{-1}\, d(a)\, \Pi \ .$$

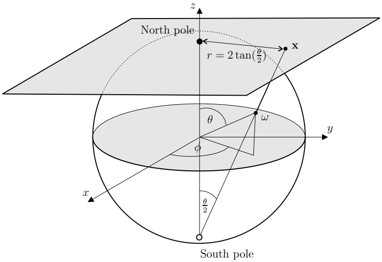

Figure: Stereographic projection.

Continuous wavelet analysis

- Wavelet frame on the sphere constructed from rotations and dilations of a mother spherical wavelet Ψ:

$$\{\Psi_{a,\rho} \equiv \mathcal{R}(\rho)\mathcal{D}(a)\Psi \, : \, \rho \in \mathrm{SO}(3), \, a \in \mathbb{R}^+_*\}.$$

- The forward wavelet transform is given by

$$W^f_\Psi(a,\rho) = \langle f, \Psi_{a,\rho} \rangle = \int_{\mathbb{S}^2} \mathrm{d}\Omega(\omega)\, f(\omega)\, \Psi^*_{a,\rho}(\omega) \,,$$

where $\mathrm{d}\Omega(\omega) = \sin\theta \, \mathrm{d}\theta \, \mathrm{d}\varphi$ is the usual invariant measure on the sphere.

- Transform general in the sense that all orientations in the rotation group $\mathrm{SO}(3)$ are considered, thus directional structure is naturally incorporated.

- Fast algorithms essential (for a review see Wiaux, McEwen & Vielva 2007)
  - Factoring of rotations: McEwen *et al.* (2007), Wandelt & Gorski (2001)
  - Separation of variables: Wiaux *et al.* (2005)

- FastCSWT code available to download: http://www.jasonmcewen.org/

Continuous wavelet analysis

- Wavelet frame on the sphere constructed from rotations and dilations of a mother spherical wavelet Ψ:

$$\{\Psi_{a,\rho} \equiv \mathcal{R}(\rho)\mathcal{D}(a)\Psi \,:\, \rho \in \mathrm{SO}(3),\, a \in \mathbb{R}^{+}_{*}\}.$$

- The forward wavelet transform is given by

$$W^{f}_{\Psi}(a,\rho) = \langle f, \Psi_{a,\rho}\rangle = \int_{\mathbb{S}^2} \mathrm{d}\Omega(\omega)\, f(\omega)\, \Psi^{*}_{a,\rho}(\omega)\ ,$$

where $\mathrm{d}\Omega(\omega) = \sin\theta\, \mathrm{d}\theta\, \mathrm{d}\varphi$ is the usual invariant measure on the sphere.

- Transform general in the sense that all orientations in the rotation group $\mathrm{SO}(3)$ are considered, thus directional structure is naturally incorporated.

- Fast algorithms essential (for a review see Wiaux, McEwen & Vielva 2007)
  - Factoring of rotations: McEwen *et al.* (2007), Wandelt & Gorski (2001)
  - Separation of variables: Wiaux *et al.* (2005)

- FastCSWT code available to download: http://www.jasonmcewen.org/

Continuous wavelet analysis

- Wavelet frame on the sphere constructed from rotations and dilations of a mother spherical wavelet Ψ:

$$\{\Psi_{a,\rho} \equiv \mathcal{R}(\rho)\mathcal{D}(a)\Psi \, : \, \rho \in \mathrm{SO}(3), \, a \in \mathbb{R}^{+}_{*}\}.$$

- The forward wavelet transform is given by

$$W^{f}_{\Psi}(a,\rho) = \langle f, \Psi_{a,\rho} \rangle = \int_{\mathbb{S}^2} \mathrm{d}\Omega(\omega) \, f(\omega) \, \Psi^{*}_{a,\rho}(\omega) \, ,$$

where $\mathrm{d}\Omega(\omega) = \sin\theta \, \mathrm{d}\theta \, \mathrm{d}\varphi$ is the usual invariant measure on the sphere.

- Transform general in the sense that all orientations in the rotation group $\mathrm{SO}(3)$ are considered, thus directional structure is naturally incorporated.

- Fast algorithms essential (for a review see Wiaux, McEwen & Vielva 2007)
  - Factoring of rotations: McEwen *et al.* (2007), Wandelt & Gorski (2001)
  - Separation of variables: Wiaux *et al.* (2005)

- FastCSWT code available to download: `http://www.jasonmcewen.org/`

Mother wavelets

- Correspondence principle between spherical and Euclidean wavelets states that the inverse stereographic projection of an *admissible* wavelet on the plane yields an *admissible* wavelet on the sphere (proved by Wiaux *et al.* 2005)

- Mother wavelets on sphere constructed from the projection of mother Euclidean wavelets defined on the plane:

$$\Psi = \Pi^{-1} \Psi_{\mathbb{R}^2} \ ,$$

 where $\Psi_{\mathbb{R}^2} \in \mathrm{L}^2(\mathbb{R}^2, \, \mathrm{d}^2 \boldsymbol{x})$ is an admissible wavelet in the plane.

- Directional wavelets on sphere may be naturally constructed in this setting – they are simply the projection of directional Euclidean planar wavelets on to the sphere.

Mother wavelets

- Correspondence principle between spherical and Euclidean wavelets states that the inverse stereographic projection of an *admissible* wavelet on the plane yields an *admissible* wavelet on the sphere (proved by Wiaux *et al.* 2005)

- Mother wavelets on sphere constructed from the projection of mother Euclidean wavelets defined on the plane:

$$\Psi = \Pi^{-1} \Psi_{\mathbb{R}^2} \, ,$$

where $\Psi_{\mathbb{R}^2} \in L^2(\mathbb{R}^2, d^2\boldsymbol{x})$ is an admissible wavelet in the plane.

- Directional wavelets on sphere may be naturally constructed in this setting – they are simply the projection of directional Euclidean planar wavelets on to the sphere.

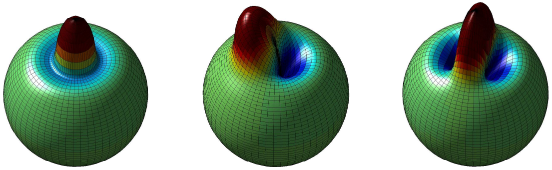

(a) SMHW (b) SBW (c) S2GDW

Figure: Spherical wavelets at scale $a, b = 0.2$.

Continuous wavelet synthesis (reconstruction)

- The inverse wavelet transform given by

$$f(\omega) = \int_0^\infty \frac{\mathrm{d}a}{a^3} \int_{\mathrm{SO}(3)} \mathrm{d}\varrho(\rho) W_\Psi^f(a, \rho) \, [\mathcal{R}(\rho)\widehat{L}_\Psi \Psi_a](\omega) \, ,$$

where $\mathrm{d}\varrho(\rho) = \sin\beta \, \mathrm{d}\alpha \, \mathrm{d}\beta \, \mathrm{d}\gamma$ is the invariant measure on the rotation group $\mathrm{SO}(3)$.

- Perfect reconstruction is ensured provided wavelets satisfy the admissibility property:

$$0 < \widehat{C}_\Psi^\ell \equiv \frac{8\pi^2}{2\ell+1} \sum_{m=-\ell}^{\ell} \int_0^\infty \frac{\mathrm{d}a}{a^3} \mid (\Psi_a)_{\ell m} \mid^2 < \infty, \quad \forall \ell \in \mathbb{N}$$

where $(\Psi_a)_{\ell m}$ are the spherical harmonic coefficients of $\Psi_a(\omega)$.

- Continuous wavelets used effectively in many cosmological studies, for example:
  - Non-Gaussianity (*e.g.* Vielva *et al.* 2004; McEwen *et al.* 2005, 2006, 2008)
  - ISW (*e.g.* Vielva *et al.* 2005, McEwen *et al.* 2007, 2008)

- BUT...

Continuous wavelet synthesis (reconstruction)

- The inverse wavelet transform given by

$$f(\omega) = \int_0^\infty \frac{\mathrm{d}a}{a^3} \int_{\mathrm{SO}(3)} \mathrm{d}\varrho(\rho) W_\Psi^f(a,\rho) \, [\mathcal{R}(\rho)\widehat{L}_\Psi \Psi_a](\omega) \, ,$$

where $\mathrm{d}\varrho(\rho) = \sin\beta \, \mathrm{d}\alpha \, \mathrm{d}\beta \, \mathrm{d}\gamma$ is the invariant measure on the rotation group $\mathrm{SO}(3)$.

- Perfect reconstruction is ensured provided wavelets satisfy the admissibility property:

$$0 < \widehat{C}_\Psi^\ell \equiv \frac{8\pi^2}{2\ell+1} \sum_{m=-\ell}^{\ell} \int_0^\infty \frac{\mathrm{d}a}{a^3} \mid (\Psi_a)_{\ell m} \mid^2 < \infty, \quad \forall \ell \in \mathbb{N}$$

where $(\Psi_a)_{\ell m}$ are the spherical harmonic coefficients of $\Psi_a(\omega)$.

- Continuous wavelets used effectively in many cosmological studies, for example:
  - Non-Gaussianity (*e.g.* Vielva *et al.* 2004; McEwen *et al.* 2005, 2006, 2008)
  - ISW (*e.g.* Vielva *et al.* 2005, McEwen *et al.* 2007, 2008)

- BUT...

Continuous wavelet synthesis (reconstruction)

- The inverse wavelet transform given by

$$f(\omega) = \int_0^\infty \frac{da}{a^3} \int_{SO(3)} d\varrho(\rho) W_\Psi^f(a, \rho) \, [\mathcal{R}(\rho) \widehat{L}_\Psi \Psi_a](\omega) \ ,$$

where $d\varrho(\rho) = \sin\beta \, d\alpha \, d\beta \, d\gamma$ is the invariant measure on the rotation group $SO(3)$.

- Perfect reconstruction is ensured provided wavelets satisfy the admissibility property:

$$0 < \widehat{C}_\Psi^\ell \equiv \frac{8\pi^2}{2\ell+1} \sum_{m=-\ell}^{\ell} \int_0^\infty \frac{da}{a^3} \mid (\Psi_a)_{\ell m} \mid^2 < \infty, \quad \forall \ell \in \mathbb{N}$$

where $(\Psi_a)_{\ell m}$ are the spherical harmonic coefficients of $\Psi_a(\omega)$.

- Continuous wavelets used effectively in many cosmological studies, for example:
  - Non-Gaussianity (*e.g.* Vielva *et al.* 2004; McEwen *et al.* 2005, 2006, 2008)
  - ISW (*e.g.* Vielva *et al.* 2005, McEwen *et al.* 2007, 2008)

- BUT... **exact reconstruction not feasible in practice!**

Continuous harmonic-dilation wavelets on the sphere

- Define dilation by scaling in harmonic space (McEwen *et al.* 2006):

$$\Psi_{\ell m}(a) = \sqrt{\frac{2\ell+1}{8\pi^2}}\,\Upsilon_m(\ell a)\ ,$$

- Wavelet analysis and synthesis defined in the same manner as stereographic wavelets.
- Admissibility condition defined on the wavelet generating functions Υ

$$0 < C_\Upsilon^\ell = \sum_{m=-\ell}^{\ell} \int_0^\infty \frac{\mathrm{d}q}{q}\,|\Upsilon_m(q)|^2 < \infty\ .$$

- Define admissible wavelet in harmonic space:

$$\Upsilon_m(\ell a) = \mathrm{e}^{-\frac{(\ell a - L)^2 + (m-M)^2}{2}} - \mathrm{e}^{-\frac{(\ell a)^2 + L^2 + (m-M)^2}{2}}\ .$$

Continuous harmonic-dilation wavelets on the sphere

- Define dilation by scaling in harmonic space (McEwen *et al.* 2006):

$$\Psi_{\ell m}(a) = \sqrt{\frac{2\ell+1}{8\pi^2}}\, \Upsilon_m(\ell a)\,,$$

- Wavelet analysis and synthesis defined in the same manner as stereographic wavelets.
- Admissibility condition defined on the wavelet generating functions Υ

$$0 < C_\Upsilon^\ell = \sum_{m=-\ell}^{\ell} \int_0^\infty \frac{\mathrm{d}q}{q}\, |\Upsilon_m(q)|^2 < \infty\,.$$

- Define admissible wavelet in harmonic space:

$$\Upsilon_m(\ell a) = \mathrm{e}^{-\frac{(\ell a - L)^2 + (m-M)^2}{2}} - \mathrm{e}^{-\frac{(\ell a)^2 + L^2 + (m-M)^2}{2}}\,.$$

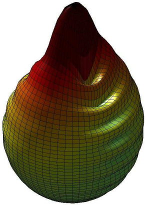

Figure: Harmonic-dilation Morlet wavelet.

Scale-discretised wavelets on the sphere

- **Exact reconstruction not feasible in practice with continuous wavelets!**
- Wiaux, McEwen, Vandergheynst, Blanc (2008)
  Exact reconstruction with directional wavelets on the sphere
  S2DW code

- Dilation performed in harmonic space.
  Following McEwen *et al.* (2006), Sanz *et al.* (2006).
- The scale-discretised wavelet $\Psi \in \mathrm{L}^2(\mathrm{S}^2, \mathrm{d}\Omega)$ is defined in harmonic space:

$$\widehat{\Psi}_{\ell m} = \tilde{K}_{\Psi}(\ell) S^{\Psi}_{\ell m} \ .$$

- Construct wavelets to satisfy a resolution of the identity for $0 \leq \ell < L$:

$$\tilde{\Phi}^2_{\Psi}(\alpha^J \ell) + \sum_{j=0}^{J} \tilde{K}^2_{\Psi}(\alpha^j \ell) = 1 \ .$$

Scale-discretised wavelets on the sphere

- **Exact reconstruction not feasible in practice with continuous wavelets!**
- Wiaux, McEwen, Vandergheynst, Blanc (2008)
  Exact reconstruction with directional wavelets on the sphere
  S2DW code

- Dilation performed in harmonic space.
  Following McEwen *et al.* (2006), Sanz *et al.* (2006).

- The scale-discretised wavelet $\Psi \in \mathrm{L}^2(\mathrm{S}^2, \mathrm{d}\Omega)$ is defined in harmonic space:

$$\widehat{\Psi}_{\ell m} = \tilde{K}_{\Psi}(\ell) S^{\Psi}_{\ell m} \ .$$

- Construct wavelets to satisfy a resolution of the identity for $0 \leq \ell < L$:

$$\tilde{\Phi}^2_{\Psi}(\alpha^J \ell) + \sum_{j=0}^{J} \tilde{K}^2_{\Psi}(\alpha^j \ell) = 1 \, .$$

Scale-discretised wavelets on the sphere

- **Exact reconstruction not feasible in practice with continuous wavelets!**
- Wiaux, McEwen, Vandergheynst, Blanc (2008)
  Exact reconstruction with directional wavelets on the sphere
  S2DW code

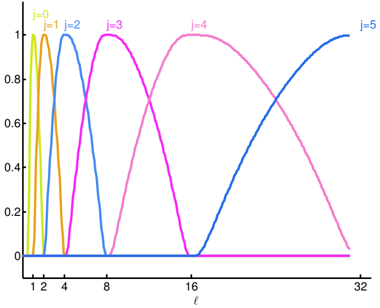

Figure: Harmonic tiling on the sphere.

- Dilation performed in harmonic space.
  Following McEwen *et al.* (2006), Sanz *et al.* (2006).
- The scale-discretised wavelet $\Psi \in \mathrm{L}^2(\mathrm{S}^2, \mathrm{d}\Omega)$ is defined in harmonic space:

$$\widehat{\Psi}_{\ell m} = \tilde{K}_\Psi(\ell) S^\Psi_{\ell m} \ .$$

- Construct wavelets to satisfy a resolution of the identity for $0 \leq \ell < L$:

$$\tilde{\Phi}^2_\Psi(\alpha^J \ell) + \sum_{j=0}^{J} \tilde{K}^2_\Psi(\alpha^j \ell) = 1 \, .$$

Scale-discretised wavelets on the sphere

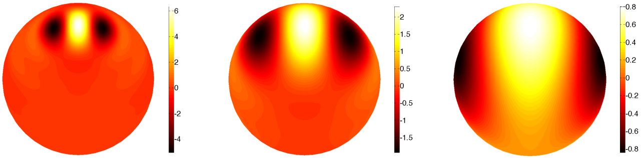

Figure: Spherical scale-discretised wavelets.

- The scale-discretised wavelet transform is given by the usual projection onto each wavelet:

$$W^f_\Psi(\rho, \alpha^j) = \langle f, \Psi_{\rho,\alpha^j} \rangle = \int_{\mathbb{S}^2} \mathrm{d}\Omega(\omega)\, f(\omega)\, \Psi^*_{\rho,\alpha^j}(\omega) \, .$$

- The original function may be recovered exactly in practice from the wavelet (and scaling) coefficients:

$$f(\omega) = [\Phi_{\alpha^J} f](\omega) + \sum_{j=0}^{J} \int_{\mathrm{SO}(3)} \mathrm{d}\varrho(\rho)\, W^f_\Psi\left(\rho, \alpha^j\right) \left[R(\rho)\, L^{\mathrm{d}} \Psi_{\alpha^j}\right](\omega) \, .$$

Scale-discretised wavelets on the sphere

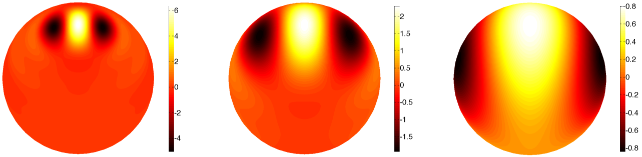

Figure: Spherical scale-discretised wavelets.

- The scale-discretised wavelet transform is given by the usual projection onto each wavelet:

$$W^f_\Psi(\rho, \alpha^j) = \langle f, \Psi_{\rho,\alpha^j} \rangle = \int_{\mathbb{S}^2} \mathrm{d}\Omega(\omega) \, f(\omega) \, \Psi^*_{\rho,\alpha^j}(\omega) \; .$$

- The original function may be recovered exactly in practice from the wavelet (and scaling) coefficients:

$$f(\omega) = [\Phi_{\alpha^J} f](\omega) + \sum_{j=0}^{J} \int_{\mathrm{SO(3)}} \mathrm{d}\varrho(\rho) \, W^f_\Psi(\rho, \alpha^j) \left[R(\rho) \, L^{\mathrm{d}} \Psi_{\alpha^j} \right](\omega) \; .$$

Scale-discretised wavelets on the sphere

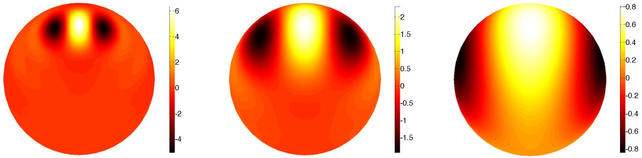

Figure: Spherical scale-discretised wavelets.

- The scale-discretised wavelet transform is given by the usual projection onto each wavelet:

$$W^f_\Psi(\rho, \alpha^j) = \langle f, \Psi_{\rho,\alpha^j} \rangle = \int_{\mathbb{S}^2} \mathrm{d}\Omega(\omega) f(\omega)\, \Psi^*_{\rho,\alpha^j}(\omega)\ .$$

- The original function may be recovered exactly in practice from the wavelet (and scaling) coefficients:

$$f(\omega) = \left[\Phi_{\alpha^J} f\right](\omega) + \sum_{j=0}^{J} \int_{\mathrm{SO}(3)} \mathrm{d}\varrho(\rho)\, W^f_\Psi\left(\rho, \alpha^j\right) \left[R(\rho) L^{\mathrm{d}} \Psi_{\alpha^j}\right](\omega)\ .$$

Scale-discretised wavelet transform of the Earth

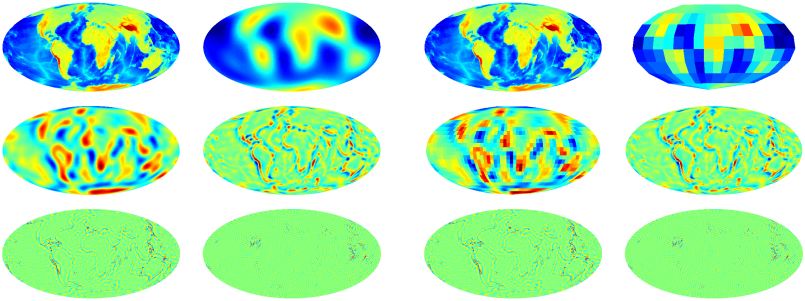

(a) Undecimated (b) Multi-resolution

Figure: Scale-discretised wavelet transform of a topography map of the Earth.

Codes to compute scale-discretised wavelets on the sphere

S2DW code

Exact reconstruction with directional wavelets on the sphere

Wiaux, McEwen, Vandergheynst, Blanc (2008)

- Fortran
- Parallelised
- Supports directional, steerable wavelets

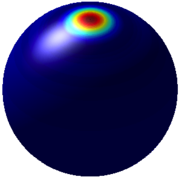

S2LET code

S2LET: A code to perform fast wavelet analysis on the sphere

Leistedt, McEwen, Vandergheynst, Wiaux (2012)

- C, Matlab, IDL, Java
- Support only axisymmetric wavelets at present
- Future extensions:
  - Directional, steerable wavelets
  - Faster algorithms to perform wavelet transforms
  - Spin wavelets

All codes available from: `http://www.jasonmcewen.org/`

Translation and convolution on the radial line

- We construct translation and convolution operators on the radial line by analogy with the infinite line.
- For the standard orthogonal basis $\phi_\omega(x) = \mathrm{e}^{\mathrm{i}\omega x}$ translation of the basis functions defined by the shift of coordinates:

$$(\mathcal{T}_u^{\mathbb{R}} \phi_\omega)(x) \equiv \phi_\omega(x-u) = \phi_\omega^*(u)\phi_\omega(x) \ .$$

- Define translation of the spherical Laguerre basis functions on the radial line by analogy:

$$(\mathcal{T}_s K_p)(r) \equiv K_p(s) K_p(r) \ .$$

- Define convolution on the radial line of by

$$(f \star h)(r) \equiv \langle f | \mathcal{T}_r h \rangle = \int_{\mathbb{R}^+} \mathrm{d}s s^2 f(s) \left(\mathcal{T}_r h\right)(s),$$

from which it follows that radial convolution in harmonic space is given by the product

$$(f \star h)_p = \langle f \star h | K_p \rangle = f_p h_p \ .$$

Translation and convolution on the radial line

- We construct translation and convolution operators on the radial line by analogy with the infinite line.
- For the standard orthogonal basis $\phi_\omega(x) = \mathrm{e}^{\mathrm{i}\omega x}$ translation of the basis functions defined by the shift of coordinates:

$$(\mathcal{T}_u^{\mathbb{R}} \phi_\omega)(x) \equiv \phi_\omega(x-u) = \phi_\omega^*(u)\phi_\omega(x) \ .$$

- Define translation of the spherical Laguerre basis functions on the radial line by analogy:

$$(\mathcal{T}_s K_p)(r) \equiv K_p(s) K_p(r) \ .$$

- Define convolution on the radial line of by

$$(f \star h)(r) \equiv \langle f | \mathcal{T}_r h \rangle = \int_{\mathbb{R}+} \mathrm{d}s s^2 f(s) \left(\mathcal{T}_r h\right)(s),$$

from which it follows that radial convolution in harmonic space is given by the product

$$(f \star h)_p = \langle f \star h | K_p \rangle = f_p h_p \ .$$

Translation and convolution on the radial line

- We construct translation and convolution operators on the radial line by analogy with the infinite line.
- For the standard orthogonal basis $\phi_\omega(x) = e^{i\omega x}$ translation of the basis functions defined by the shift of coordinates:

$$(\mathcal{T}_u^{\mathbb{R}} \phi_\omega)(x) \equiv \phi_\omega(x-u) = \phi_\omega^*(u)\phi_\omega(x) \ .$$

- Define translation of the spherical Laguerre basis functions on the radial line by analogy:

$$(\mathcal{T}_s K_p)(r) \equiv K_p(s)K_p(r) \ .$$

- Define convolution on the radial line of by

$$(f \star h)(r) \equiv \langle f | \mathcal{T}_r h \rangle = \int_{\mathbb{R}+} \mathrm{d}s s^2 f(s) \left(\mathcal{T}_r h\right)(s),$$

from which it follows that radial convolution in harmonic space is given by the product

$$(f \star h)_p = \langle f \star h | K_p \rangle = f_p h_p \ .$$

Translation and convolution on the radial line

- Translation corresponds to convolution with the Dirac delta:

$$(f \star \delta_s)(r) = \sum_{p=0}^{\infty} f_p K_p(s) K_p(r) = (\mathcal{T}_s f)(r) \ .$$

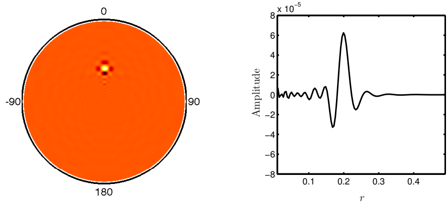

(a) Wavelet kernel translated by $r = 0.2$

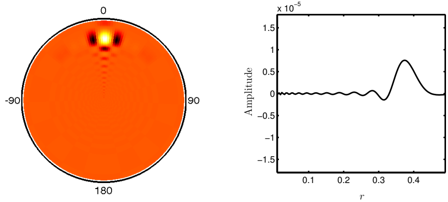

(b) Wavelet kernel translated by $r = 0.4$

Scale-discretised wavelets on the ball

- *Exact wavelets on the ball* (Leistedt & McEwen 2012).
- Define translation and convolution operators on the radial line.
- Dilation performed in harmonic space.
- Scale-discretised wavelet $\Psi \in \mathrm{L}^2(B^3)$ is defined in harmonic space:

$$\Psi^{jj'}_{\ell m p} \equiv \sqrt{\frac{2\ell+1}{4\pi}}\, \kappa_\lambda\left(\frac{\ell}{\lambda^j}\right) \kappa_\nu\left(\frac{p}{\nu^{j'}}\right) \delta_{m0}\,.$$

- Construct wavelets to satisfy a resolution of the identity:

$$\frac{4\pi}{2\ell+1}\left(|\Phi_{\ell 0 p}|^2 + \sum_{j=J_0}^{J} \sum_{j'=J'_0}^{J'} |\Psi^{jj'}_{\ell 0 p}|^2 \right) = 1, \;\forall \ell, p.$$

Scale-discretised wavelets on the ball

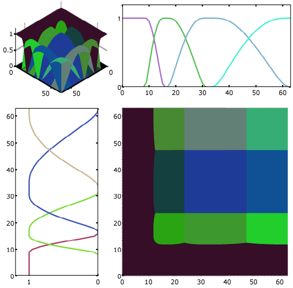

Figure: Tiling of Fourier-Laguerre space.

- *Exact wavelets on the ball* (Leistedt & McEwen 2012).
- Define translation and convolution operators on the radial line.
- Dilation performed in harmonic space.
- Scale-discretised wavelet $\Psi \in \mathrm{L}^2(B^3)$ is defined in harmonic space:

$$\Psi^{jj'}_{\ell m p} \equiv \sqrt{\frac{2\ell+1}{4\pi}} \, \kappa_\lambda\left(\frac{\ell}{\lambda^j}\right) \kappa_\nu\left(\frac{p}{\nu^{j'}}\right) \delta_{m0} \, .$$

- Construct wavelets to satisfy a resolution of the identity:

$$\frac{4\pi}{2\ell+1}\left(|\Phi_{\ell 0 p}|^2 + \sum_{j=J_0}^{J} \sum_{j'=J'_0}^{J'} |\Psi^{jj'}_{\ell 0 p}|^2 \right) = 1, \ \forall \ell, p .$$

Scale-discretised wavelets on the ball

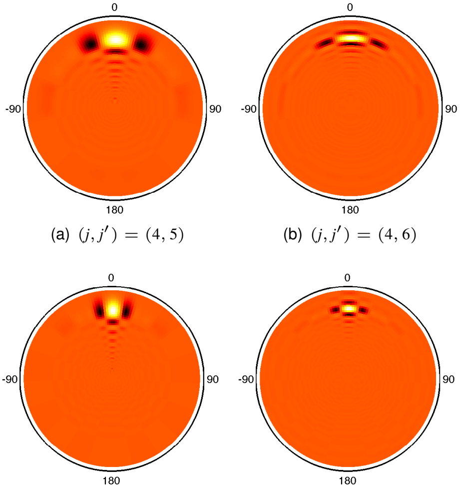

(a) $(j, j') = (4, 5)$

(b) $(j, j') = (4, 6)$

(c) $(j, j') = (5, 5)$

(d) $(j, j') = (5, 6)$

Figure: Scale-discretised wavelets on the ball.

Scale-discretised wavelets on the ball

- The scale-discretised wavelet transform is given by the usual projection onto each wavelet:

$$W^{\Psi^{jj'}}(\boldsymbol{r}) \equiv (f \star \Psi^{jj'})(\boldsymbol{r}) = \langle f | \mathcal{T}_r \mathcal{R}_\omega \Psi^{jj'} \rangle \ .$$

- The original function may be recovered exactly in practice from the wavelet (and scaling) coefficients:

$$f(\boldsymbol{r}) = \int_{B^3} \mathrm{d}^3\boldsymbol{r}' \, W^{\Phi}(\boldsymbol{r}')(\mathcal{T}_r \mathcal{R}_\omega \Phi)(\boldsymbol{r}') + \sum_{j=J_0}^{J} \sum_{j'=J_0'}^{J'} \int_{B^3} \mathrm{d}^3\boldsymbol{r}' \, W^{\Psi^{jj'}}(\boldsymbol{r}')(\mathcal{T}_r \mathcal{R}_\omega \Psi^{jj'})(\boldsymbol{r}') \ .$$

Scale-discretised wavelet denoising on the ball

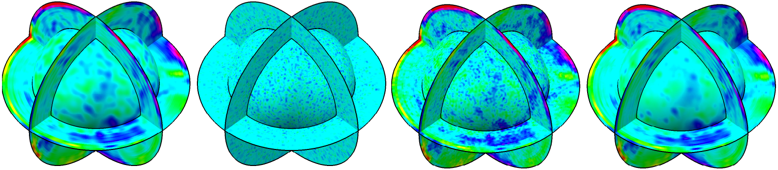

(a) Ground truth (b) Noise (c) Noisy (SNR=5dB) (d) Denoised (SNR=17dB)

Figure: Denoising of a seismological Earth model.

Scale-discretised wavelet denoising on the ball

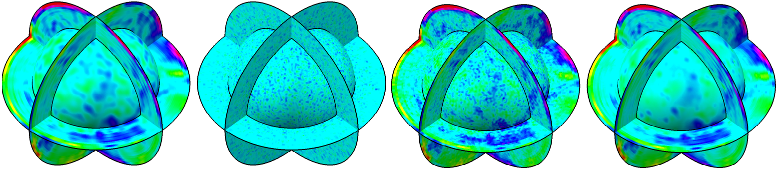

(a) Ground truth (b) Noise (c) Noisy (SNR=5dB) (d) Denoised (SNR=17dB)

Figure: Denoising of a seismological Earth model.

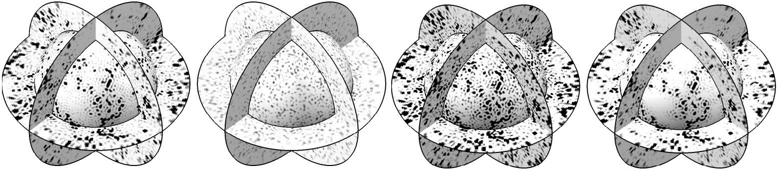

(a) Ground truth (b) Noise (c) Noisy (SNR=5dB) (d) Denoised (SNR=11dB)

Figure: Denoising of an N-body simulation.

Codes for scale-discretised wavelet on the ball

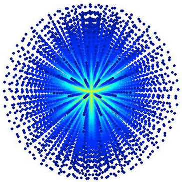

FLAG code
Exact wavelets on the ball
Leistedt & McEwen (2012)

- C, Matlab, IDL, Java
- Exact Fourier-LAGuerre transform on the ball

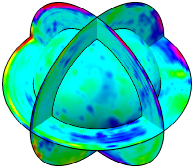

FLAGLET code
Exact wavelets on the ball
Leistedt & McEwen (2012)

- C, Matlab, IDL, Java
- Exact (Fourier-LAGuerre) wavelets on the ball – coined *flaglets*!

All codes available from: http://www.jasonmcewen.org/

Outline

An introduction to compressive sensing

- **"Nothing short of revolutionary."**
  – National Science Foundation
- Developed by Emmanuel Candes and David Donoho (and others).

(a) Emmanuel Candes

(b) David Donoho

An introduction to compressive sensing

- Next evolution of wavelet analysis → wavelets are a key ingredient.
- Move compression to the acquisition stage → compressive sensing.
- Acquisition versus imaging.

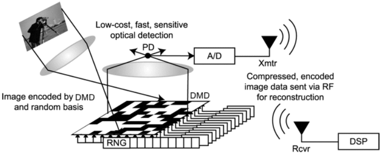

(a) Architecture

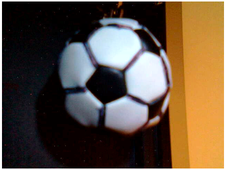

(b) Scene

(c) Recov. (20% meas.)

Figure: Single pixel camera

An introduction to compressive sensing

- Next evolution of wavelet analysis → wavelets are a key ingredient.
- Move compression to the acquisition stage → compressive sensing.
- Acquisition versus imaging.

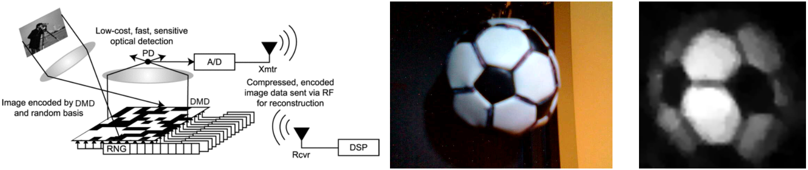

(a) Architecture (b) Scene (c) Recov. (20% meas.)

Figure: Single pixel camera

An introduction to compressive sensing

- Ill-posed inverse problem:

$$\boldsymbol{y} = \Phi \boldsymbol{x} + \boldsymbol{n} = \Phi \Psi \boldsymbol{\alpha} + \boldsymbol{n} .$$

- Solve by imposing a regularising prior that the signal to be recovered is sparse in Ψ, *i.e.* solve the following ℓ_0 optimisation problem:

$$\boldsymbol{\alpha}^\star = \arg\min_{\boldsymbol{\alpha}} \|\alpha\|_0 \text{ such that } \|\boldsymbol{y} - \Phi\Psi\boldsymbol{\alpha}\|_2 \leq \epsilon ,$$

where the signal is synthesising by $\boldsymbol{x}^\star = \Psi \boldsymbol{\alpha}^\star$.

- Recall norms given by:

$$\|\alpha\|_0 = \text{no. non-zero elements} \qquad \|\alpha\|_1 = \sum_i |\alpha_i| \qquad \|\alpha\|_2 = \Big(\sum_i |\alpha_i|^2\Big)^{1/2}$$

- Solving this problem is difficult (combinatorial).

- Instead, solve the ℓ_1 optimisation problem (convex):

$$\boldsymbol{\alpha}^\star = \arg\min_{\boldsymbol{\alpha}} \|\alpha\|_1 \text{ such that } \|\boldsymbol{y} - \Phi\Psi\boldsymbol{\alpha}\|_2 \leq \epsilon .$$

An introduction to compressive sensing

- Ill-posed inverse problem:

$$\boldsymbol{y} = \Phi \boldsymbol{x} + \boldsymbol{n} = \Phi \Psi \boldsymbol{\alpha} + \boldsymbol{n} .$$

- Solve by imposing a regularising prior that the signal to be recovered is sparse in Ψ, *i.e.* solve the following ℓ_0 optimisation problem:

$$\boldsymbol{\alpha}^\star = \underset{\boldsymbol{\alpha}}{\arg\min} \|\alpha\|_0 \text{ such that } \|\boldsymbol{y} - \Phi\Psi\boldsymbol{\alpha}\|_2 \leq \epsilon ,$$

where the signal is synthesising by $\boldsymbol{x}^\star = \Psi \boldsymbol{\alpha}^\star$.

- Recall norms given by:

$$\|\alpha\|_0 = \text{no. non-zero elements} \qquad \|\alpha\|_1 = \sum_i |\alpha_i| \qquad \|\alpha\|_2 = \Big(\sum_i |\alpha_i|^2\Big)^{1/2}$$

- Solving this problem is difficult (combinatorial).
- Instead, solve the ℓ_1 optimisation problem (convex):

$$\boldsymbol{\alpha}^\star = \underset{\boldsymbol{\alpha}}{\arg\min} \|\alpha\|_1 \text{ such that } \|\boldsymbol{y} - \Phi\Psi\boldsymbol{\alpha}\|_2 \leq \epsilon .$$

An introduction to compressive sensing

- Ill-posed inverse problem:

$$\boldsymbol{y} = \Phi \boldsymbol{x} + \boldsymbol{n} = \Phi \Psi \boldsymbol{\alpha} + \boldsymbol{n} .$$

- Solve by imposing a regularising prior that the signal to be recovered is sparse in Ψ, *i.e.* solve the following ℓ_0 optimisation problem:

$$\boldsymbol{\alpha}^\star = \arg\min_{\boldsymbol{\alpha}} \|\alpha\|_0 \text{ such that } \|\boldsymbol{y} - \Phi\Psi\boldsymbol{\alpha}\|_2 \leq \epsilon ,$$

where the signal is synthesising by $\boldsymbol{x}^\star = \Psi \boldsymbol{\alpha}^\star$.

- Recall norms given by:

$$\|\alpha\|_0 = \text{no. non-zero elements} \qquad \|\alpha\|_1 = \sum_i |\alpha_i| \qquad \|\alpha\|_2 = \Big(\sum_i |\alpha_i|^2\Big)^{1/2}$$

- Solving this problem is difficult (combinatorial).
- Instead, solve the ℓ_1 optimisation problem (convex):

$$\boldsymbol{\alpha}^\star = \arg\min_{\boldsymbol{\alpha}} \|\alpha\|_1 \text{ such that } \|\boldsymbol{y} - \Phi\Psi\boldsymbol{\alpha}\|_2 \leq \epsilon .$$

An introduction to compressive sensing

- The solutions of the ℓ_0 and ℓ_1 problems are often the same.
- Restricted isometry property (RIP):

$$(1-\delta_K)\|\boldsymbol{\alpha}\|_2^2 \leq \|\Theta\boldsymbol{\alpha}\|_2^2 \leq (1+\delta_K)\|\boldsymbol{\alpha}\|_2^2 \,,$$

for K-sparse $\boldsymbol{\alpha}$, where $\Theta = \Phi\Psi$.

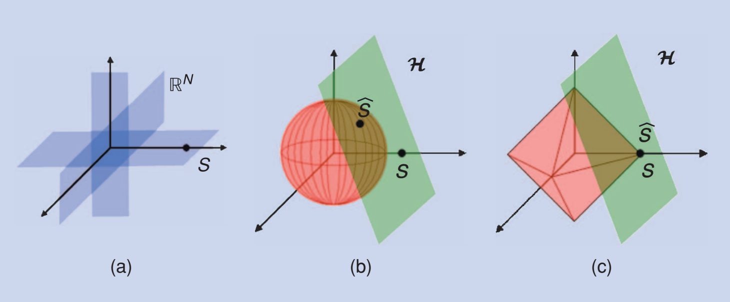

Figure: Geometry of (a) ℓ_0 (b) ℓ_2 and (c) ℓ_1 problems. [Credit: Baraniuk (2007)]

Sparse signal reconstruction on the sphere

- Consider sparse reconstruction on the sphere.
- More efficient sampling theorem $\rightarrow$ implications for sparse signal reconstruction.
  - Improves both the dimensionality and sparsity signals in the spatial domain.
  - Improves the fidelity of sparse signal reconstruction.
- Consider the inverse problem

$$\boldsymbol{y} = \Phi \boldsymbol{x} + \boldsymbol{n}$$

where:
  - $\boldsymbol{x} \in \mathbb{R}^N$ denotes the samples of f;
  - N is the number of samples on the sphere of the adopted sampling theorem;
  - $\Phi \in \mathbb{R}^{M \times N}$ denotes the measurement operator, representing a random masking of the signal;
  - M noisy measurements $\boldsymbol{y} \in \mathbb{R}^M$ are acquired;
  - $\boldsymbol{n} \in \mathbb{R}^M$ denotes iid Gaussian noise with zero mean.

Sparse signal reconstruction on the sphere

- Consider sparse reconstruction on the sphere.
- More efficient sampling theorem $\rightarrow$ implications for sparse signal reconstruction.
  - Improves both the dimensionality and sparsity signals in the spatial domain.
  - Improves the fidelity of sparse signal reconstruction.
- Consider the inverse problem

$$\boxed{\boldsymbol{y} = \Phi \boldsymbol{x} + \boldsymbol{n}}$$

where:

  - $\boldsymbol{x} \in \mathbb{R}^N$ denotes the samples of f;
  - N is the number of samples on the sphere of the adopted sampling theorem;
  - $\Phi \in \mathbb{R}^{M \times N}$ denotes the measurement operator, representing a random masking of the signal;
  - M noisy measurements $\boldsymbol{y} \in \mathbb{R}^M$ are acquired;
  - $\boldsymbol{n} \in \mathbb{R}^M$ denotes iid Gaussian noise with zero mean.

TV inpainting on the sphere

- Develop a framework for total variation (TV) inpainting on the sphere as illustrative example to study implications of sampling theorems (McEwen *et al.* 2013).

- Define TV norm on the sphere:

$$\int_{\mathbb{S}^2} \mathrm{d}\Omega \, |\nabla f| \simeq \sum_{t=0}^{N_\theta - 1} \sum_{p=0}^{N_\varphi - 1} |\nabla f| \, q(\theta_t) \simeq \sum_{t=0}^{N_\theta - 1} \sum_{p=0}^{N_\varphi - 1} \sqrt{q^2(\theta_t)(\delta_\theta \boldsymbol{x})^2 + \frac{q^2(\theta_t)}{\sin^2\theta_t}(\delta_\varphi \boldsymbol{x})^2} \equiv \|\boldsymbol{x}\|_{\mathrm{TV},\mathbb{S}^2} \, .$$

- TV inpainting problem solved directly on the sphere:

$$\boldsymbol{x}^\star = \arg\min_{\boldsymbol{x}} \|\boldsymbol{x}\|_{\mathrm{TV},\mathbb{S}^2} \quad \text{such that} \quad \|\boldsymbol{y} - \Phi \boldsymbol{x}\|_2 \leq \epsilon \, .$$

- TV inpainting problem solved in harmonic space:

$$\hat{\boldsymbol{x}}'^\star = \arg\min_{\hat{\boldsymbol{x}}} \|\Lambda \hat{\boldsymbol{x}}\|_{\mathrm{TV},\mathbb{S}^2} \quad \text{such that} \quad \|\boldsymbol{y} - \Phi \Lambda \hat{\boldsymbol{x}}\|_2 \leq \epsilon \, ,$$

  where Λ represents the inverse spherical harmonic transform.

- Solve using convex optimisation techniques adapted to the sphere (Douglas-Rachford splitting).

TV inpainting on the sphere

- Develop a framework for total variation (TV) inpainting on the sphere as illustrative example to study implications of sampling theorems (McEwen *et al.* 2013).

- Define TV norm on the sphere:

$$\int_{\mathbb{S}^2} \mathrm{d}\Omega \, |\nabla f| \simeq \sum_{t=0}^{N_\theta - 1} \sum_{p=0}^{N_\varphi - 1} |\nabla f| \, q(\theta_t) \simeq \sum_{t=0}^{N_\theta - 1} \sum_{p=0}^{N_\varphi - 1} \sqrt{q^2(\theta_t)(\delta_\theta \boldsymbol{x})^2 + \frac{q^2(\theta_t)}{\sin^2 \theta_t}(\delta_\varphi \boldsymbol{x})^2} \equiv \|\boldsymbol{x}\|_{\mathrm{TV},\mathbb{S}^2} .$$

- TV inpainting problem solved directly on the sphere:

$$\boldsymbol{x}^\star = \underset{\boldsymbol{x}}{\arg\min} \, \|\boldsymbol{x}\|_{\mathrm{TV},\mathbb{S}^2} \quad \text{such that} \quad \|\boldsymbol{y} - \Phi \boldsymbol{x}\|_2 \leq \epsilon .$$

- TV inpainting problem solved in harmonic space:

$$\hat{\boldsymbol{x}}'^\star = \underset{\hat{\boldsymbol{x}}}{\arg\min} \, \|\Lambda \hat{\boldsymbol{x}}\|_{\mathrm{TV},\mathbb{S}^2} \quad \text{such that} \quad \|\boldsymbol{y} - \Phi \Lambda \hat{\boldsymbol{x}}\|_2 \leq \epsilon ,$$

  where Λ represents the inverse spherical harmonic transform.

- Solve using convex optimisation techniques adapted to the sphere (Douglas-Rachford splitting).

TV inpainting on the sphere

- Develop a framework for total variation (TV) inpainting on the sphere as illustrative example to study implications of sampling theorems (McEwen *et al.* 2013).
- Define TV norm on the sphere:

$$\int_{\mathbb{S}^2} \mathrm{d}\Omega \, |\nabla f| \simeq \sum_{t=0}^{N_\theta - 1} \sum_{p=0}^{N_\varphi - 1} |\nabla f| \, q(\theta_t) \simeq \sum_{t=0}^{N_\theta - 1} \sum_{p=0}^{N_\varphi - 1} \sqrt{q^2(\theta_t)(\delta_\theta \boldsymbol{x})^2 + \frac{q^2(\theta_t)}{\sin^2 \theta_t}(\delta_\varphi \boldsymbol{x})^2} \equiv \|\boldsymbol{x}\|_{\mathrm{TV},\mathbb{S}^2} \, .$$

- TV inpainting problem solved directly on the sphere:

$$\boldsymbol{x}^\star = \arg\min_{\boldsymbol{x}} \|\boldsymbol{x}\|_{\mathrm{TV},\mathbb{S}^2} \text{ such that } \|\boldsymbol{y} - \Phi \boldsymbol{x}\|_2 \leq \epsilon \, .$$

- TV inpainting problem solved in harmonic space:

$$\hat{\boldsymbol{x}}'^\star = \arg\min_{\hat{\boldsymbol{x}}} \|\Lambda \hat{\boldsymbol{x}}\|_{\mathrm{TV},\mathbb{S}^2} \text{ such that } \|\boldsymbol{y} - \Phi \Lambda \hat{\boldsymbol{x}}\|_2 \leq \epsilon \, ,$$

  where Λ represents the inverse spherical harmonic transform.
- Solve using convex optimisation techniques adapted to the sphere (Douglas-Rachford splitting).

TV inpainting: low-resolution simulations

- Solve TV inpainting problem on the sphere in the context of the Driscoll & Healy (1994) and the McEwen & Wiaux (2011) sampling theorems (at $L = 32$).

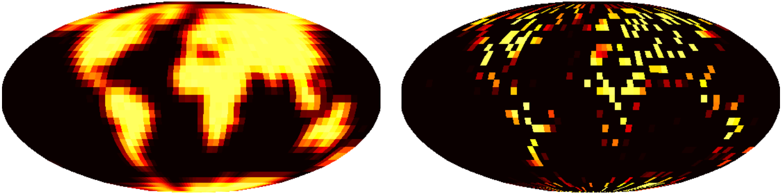

(a) Ground truth (b) Measurements

Figure: Earth topographic data reconstructed in the harmonic domain for $M/2L^2 = 1/4$

TV inpainting: low-resolution simulations

- Solve TV inpainting problem on the sphere in the context of the Driscoll & Healy (1994) and the McEwen & Wiaux (2011) sampling theorems (at $L = 32$).

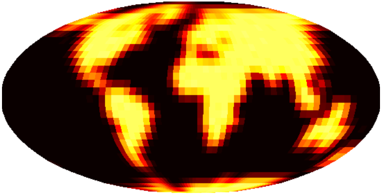

(a) Ground truth

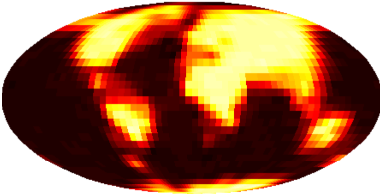

(b) DH reconstruction

Figure: Earth topographic data reconstructed in the harmonic domain for $M/2L^2 = 1/4$

TV inpainting: low-resolution simulations

- Solve TV inpainting problem on the sphere in the context of the Driscoll & Healy (1994) and the McEwen & Wiaux (2011) sampling theorems (at $L = 32$).

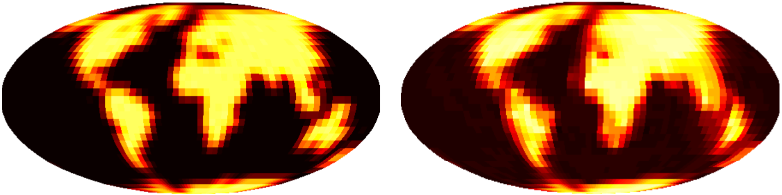

(a) Ground truth (b) MW reconstruction

Figure: Earth topographic data reconstructed in the harmonic domain for $M/2L^2 = 1/4$

TV inpainting: low-resolution simulations

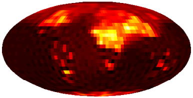
(a) DH spatial for $\frac{M}{L^2} = \frac{1}{4}$


(b) DH harmonic for $\frac{M}{L^2} = \frac{1}{4}$

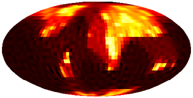
(c) MW spatial for $\frac{M}{L^2} = \frac{1}{4}$

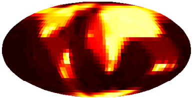
(d) MW harmonic for $\frac{M}{L^2} = \frac{1}{4}$

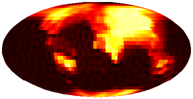
(e) DH spatial for $\frac{M}{L^2} = \frac{1}{2}$

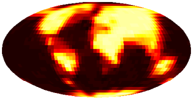
(f) DH harmonic for $\frac{M}{L^2} = \frac{1}{2}$

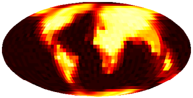
(g) MW spatial for $\frac{M}{L^2} = \frac{1}{2}$

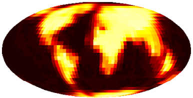
(h) MW harmonic for $\frac{M}{L^2} = \frac{1}{2}$

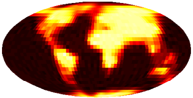
(i) DH spatial for $\frac{M}{L^2} = 1$

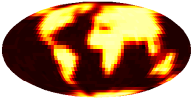
(j) DH harmonic for $\frac{M}{L^2} = 1$

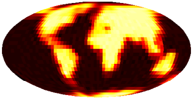
(k) MW spatial for $\frac{M}{L^2} = 1$

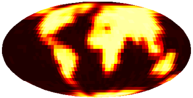
(l) MW harmonic for $\frac{M}{L^2} = 1$

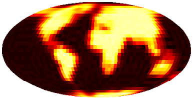
(m) DH spatial for $\frac{M}{L^2} = \frac{3}{2}$

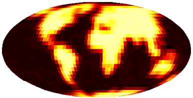
(n) DH harmonic for $\frac{M}{L^2} = \frac{3}{2}$

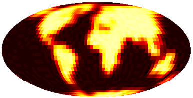
(o) MW spatial for $\frac{M}{L^2} = \frac{3}{2}$

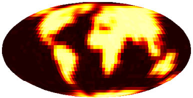
(p) MW harmonic for $\frac{M}{L^2} = \frac{3}{2}$

TV inpainting: low-resolution simulations

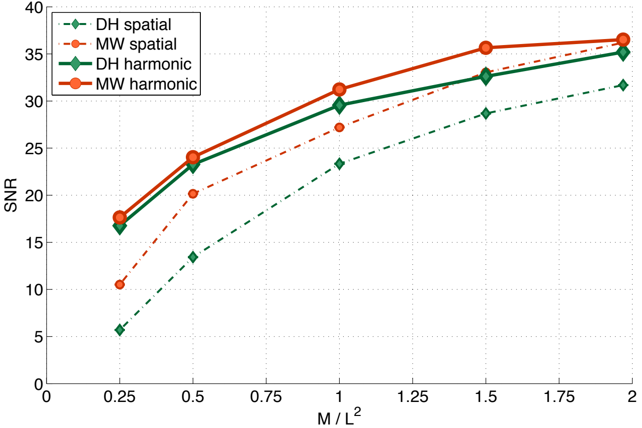

Figure: Reconstruction performance for the DH and MW sampling theorems

TV inpainting: high-resolution simulations

- Previously limited to low-resolution simulations.
- To solve high-resolution problem we require fast adjoint spherical harmonic transform operators in addition to fast forward spherical harmonic transforms to solve optimisation problems.
- Develop fast adjoints for the McEwen & Wiaux (2011) sampling theorem only.

Fast adjoint inverse spherical harmonic transform

$$ {}_s\tilde{f}^{\dagger}(\theta_t, \varphi_p) = \begin{cases} {}_sf(\theta_t, \varphi_p)\,, & t \in \{0, 1, \dots, L-1\} \\ 0\,, & t \in \{L, \dots, 2L-2\} \end{cases} $$

$$ {}_sF_{mm'}{}^{\dagger} = \sum_{t=0}^{2L-2} \sum_{p=0}^{2L-2} {}_s\tilde{f}^{\dagger}(\theta_t, \varphi_p)\, \mathrm{e}^{-\mathrm{i}(m'\theta_t + m\varphi_p)} $$

$$ {}_sf_{\ell m}{}^{\dagger} = (-1)^s\, \mathrm{i}^{m+s} \sqrt{\frac{2\ell+1}{4\pi}} \sum_{m'=-(L-1)}^{L-1} \Delta^{\ell}_{m'm}\, \Delta^{\ell}_{m',-s}\; {}_sF_{mm'}{}^{\dagger} $$

TV inpainting: high-resolution simulations

Fast adjoint forward spherical harmonic transform

$$ {}_sG_{mm'}{}^{\dagger} \;=\; (-1)^s \,\mathrm{i}^{-(m+s)} \sum_{\ell=0}^{L-1} \sqrt{\frac{2\ell+1}{4\pi}}\; \Delta^{\ell}_{m'm}\, \Delta^{\ell}_{m',-s}\; {}_sf_{\ell m} $$

$$ {}_sF_{mm''}{}^{\dagger} = 2\pi \sum_{m'=-(L-1)}^{L-1} {}_sG_{mm'}{}^{\dagger}\, w(m'-m'') $$

$$ {}_s\tilde{F}_m{}^{\dagger}(\theta_t) = \frac{1}{2L-1} \sum_{m'=-(L-1)}^{L-1} {}_sF_{mm'}{}^{\dagger}\, \mathrm{e}^{\mathrm{i}m'\theta_t} $$

$$ {}_sF_m{}^{\dagger}(\theta_t) = \begin{cases} {}_s\tilde{F}_m{}^{\dagger}(\theta_t) + (-1)^{m+s}\, {}_s\tilde{F}_m{}^{\dagger}(\theta_{2L-2-t}) \,, & t \in \{0,1,\dots,L-2\} \\ {}_s\tilde{F}_m{}^{\dagger}(\theta_t) \,, & t = L-1 \end{cases} $$

$$ {}_sf^{\dagger}(\theta_t,\varphi_p) = \frac{1}{2L-1} \sum_{m=-(L-1)}^{L-1} {}_sF_m{}^{\dagger}(\theta_t)\, \mathrm{e}^{\mathrm{i}m\varphi_p} $$

TV inpainting: high-resolution simulations

- Using fast adjoints we solve high-resolution TV inpainting problem with realistic data.

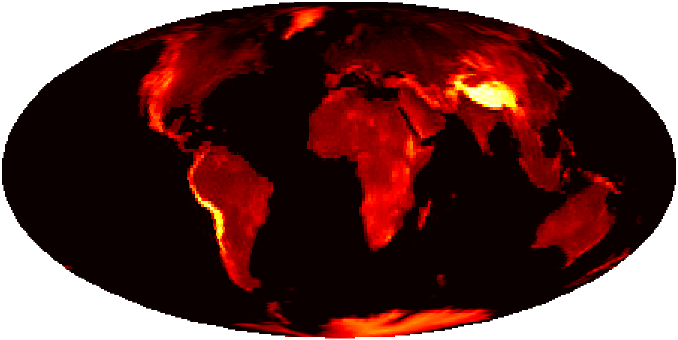

Figure: Ground truth at $L = 128$.

TV inpainting: high-resolution simulations

- Using fast adjoints we solve high-resolution TV inpainting problem with realistic data.

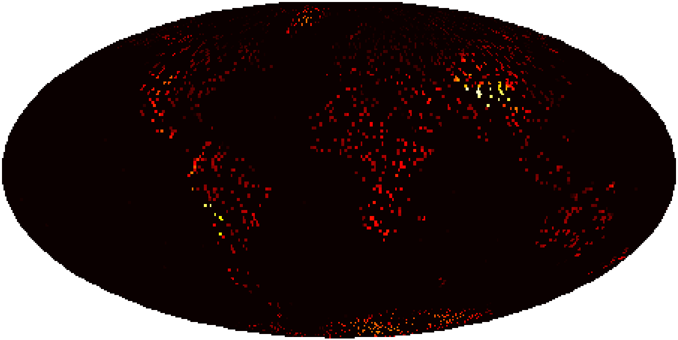

Figure: Measurements at $L = 128$ for $M/2L^2 = 1/8$.

TV inpainting: high-resolution simulations

- Using fast adjoints we solve high-resolution TV inpainting problem with realistic data.

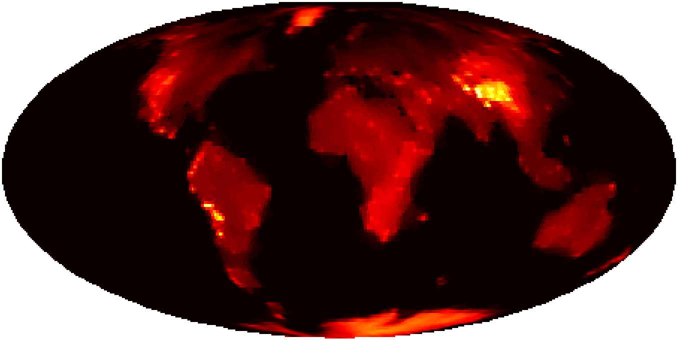

Figure: MW reconstruction in the harmonic domain at $L = 128$ for $M/2L^2 = 1/8$ ($\mathrm{SNR_I} = 20$dB).

Future extensions

- Perform sparse signal recovery on the sphere using wavelets Ψ.
- Consider the synthesis-based framework:

$$\boldsymbol{\alpha}^\star = \underset{\boldsymbol{\alpha}}{\arg\min} \, \|\boldsymbol{\alpha}\|_{1,\mathbb{S}^2} \text{ such that } \|\boldsymbol{y} - \Phi\Psi\boldsymbol{\alpha}\|_2 \leq \epsilon \, .$$

  where we synthesise the signal from its recovered wavelet coefficients by $\boldsymbol{x}^\star = \Psi\boldsymbol{\alpha}^\star$.

- Consider the analysis-based framework:

$$\boldsymbol{x}^\star = \underset{\boldsymbol{x}}{\arg\min} \, \|\Psi^{\mathrm{T}}\boldsymbol{x}\|_{1,\mathbb{S}^2} \text{ such that } \|\boldsymbol{y} - \Phi\boldsymbol{x}\|_2 \leq \epsilon \, ,$$

  where the signal $\boldsymbol{x}^\star$ is recovered directly.

- Concatenating dictionaries (Rauhut *et al.* 2008) and sparsity averaging (Carrillo, McEwen & Wiaux 2013)

$$\Psi = [\Psi_1, \Psi_2, \cdots, \Psi_q] \, .$$

- Dictionary learning (*cf.* Aharon *et al.* 2006).

Future extensions

- Perform sparse signal recovery on the sphere using wavelets Ψ.
- Consider the synthesis-based framework:

$$\boldsymbol{\alpha}^\star = \underset{\boldsymbol{\alpha}}{\arg\min} \, \|\boldsymbol{\alpha}\|_{1,\mathbb{S}^2} \;\text{ such that }\; \|\boldsymbol{y} - \Phi\Psi\boldsymbol{\alpha}\|_2 \leq \epsilon \,.$$

  where we synthesise the signal from its recovered wavelet coefficients by $\boldsymbol{x}^\star = \Psi\boldsymbol{\alpha}^\star$.

- Consider the analysis-based framework:

$$\boldsymbol{x}^\star = \underset{\boldsymbol{x}}{\arg\min} \, \|\Psi^{\mathrm{T}}\boldsymbol{x}\|_{1,\mathbb{S}^2} \;\text{ such that }\; \|\boldsymbol{y} - \Phi\boldsymbol{x}\|_2 \leq \epsilon \,,$$

  where the signal $\boldsymbol{x}^\star$ is recovered directly.

- Concatenating dictionaries (Rauhut *et al.* 2008) and sparsity averaging (Carrillo, McEwen & Wiaux 2013)

$$\Psi = [\Psi_1, \Psi_2, \cdots, \Psi_q] \,.$$

- Dictionary learning (*cf.* Aharon *et al.* 2006).

Outline

Cosmic structure

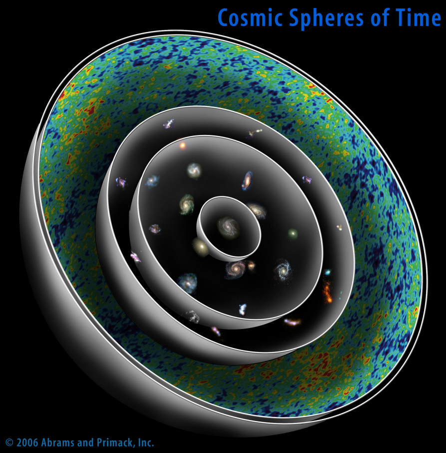

Cosmic strings

- Symmetry breaking phase transitions in the early Universe $\rightarrow$ topological defects.
- Cosmic strings well-motivated phenomenon that arise when axial or cylindrical symmetry is broken $\rightarrow$ line-like discontinuities in the fabric of the Universe.
- Although we have not yet observed cosmic strings, we have observed string-like topological defects in other media, e.g. ice and liquid crystal.
- Cosmic strings are distinct to the fundamental superstrings of string theory.
- However, recent developments in string theory suggest the existence of macroscopic superstrings that could play a similar role to cosmic strings.
- The detection of cosmic strings would open a new window into the physics of the Universe!

Figure: Optical microscope photograph of a thin film of freely suspended nematic liquid crystal after a temperature quench. [Credit: Chuang *et al.* (1991).]

Cosmic strings

- Symmetry breaking phase transitions in the early Universe → topological defects.
- Cosmic strings well-motivated phenomenon that arise when axial or cylindrical symmetry is broken → line-like discontinuities in the fabric of the Universe.
- Although we have not yet observed cosmic strings, we have observed string-like topological defects in other media, e.g. ice and liquid crystal.
- Cosmic strings are distinct to the fundamental superstrings of string theory.
- However, recent developments in string theory suggest the existence of macroscopic superstrings that could play a similar role to cosmic strings.
- The detection of cosmic strings would open a new window into the physics of the Universe!

Figure: Optical microscope photograph of a thin film of freely suspended nematic liquid crystal after a temperature quench. [Credit: Chuang *et al.* (1991).]

Cosmic strings

- Symmetry breaking phase transitions in the early Universe → topological defects.
- Cosmic strings well-motivated phenomenon that arise when axial or cylindrical symmetry is broken → line-like discontinuities in the fabric of the Universe.
- Although we have not yet observed cosmic strings, we have observed string-like topological defects in other media, e.g. ice and liquid crystal.
- Cosmic strings are distinct to the fundamental superstrings of string theory.
- However, recent developments in string theory suggest the existence of macroscopic superstrings that could play a similar role to cosmic strings.
- The detection of cosmic strings would open a new window into the physics of the Universe!

Figure: Optical microscope photograph of a thin film of freely suspended nematic liquid crystal after a temperature quench. [Credit: Chuang *et al.* (1991).]

Observational signatures of cosmic strings

- Spacetime about a cosmic string is canonical, with a three-dimensional wedge removed (Vilenkin 1981).
- Strings moving transverse to the line of sight induce line-like discontinuities in the CMB (Kaiser & Stebbins 1984).
- The amplitude of the induced contribution scales with $G\mu$, the string tension.

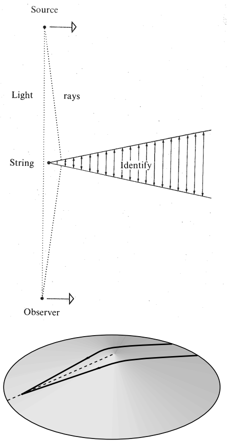

Spacetime around a cosmic string. [Credit: Kaiser & Stebbins 1984, DAMTP.]

Observational signatures of cosmic strings

- Make contact between theory and data using high-resolution simulations.
- Amplitude of the signal is given by the string tension $G\mu$.
- Search for a weak string signal s embedded in the CMB c, with observations d given by

$$d = c + s\,.$$

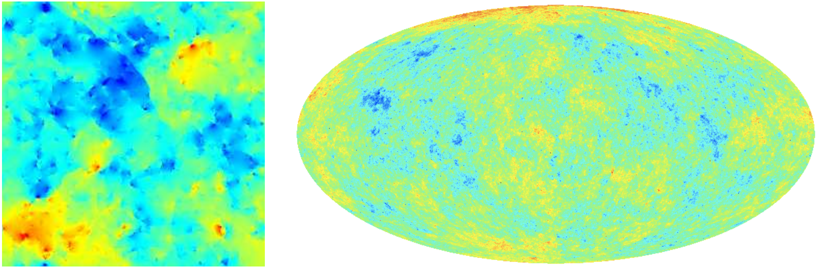

(a) Flat patch (Fraisse *et al.* 2008) (b) Full-sky (Ringeval *et al.* 2012)

Figure: Cosmic string simulations.

Motivation for using wavelets to detect cosmic strings

- Adopt the scale-discretised wavelet transform on the sphere (Wiaux, McEwen *et al.* 2008), where we denote the wavelet coefficients of the data d by $\boxed{W^d_{j\rho} = \langle d,\ \Psi_{j\rho} \rangle}$ for scale $j \in \mathbb{Z}^+$ and position $\rho \in \mathrm{SO}(3)$.
- Consider an even azimuthal band-limit $N = 4$ to yield wavelet with odd azimuthal symmetry.

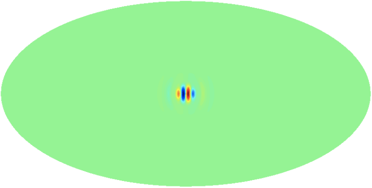

Figure: Example wavelet.

- Wavelet transform yields a sparse representation of the string signal $\rightarrow$ hope to effectively separate the CMB and string signal in wavelet space.

Motivation for using wavelets to detect cosmic strings

- Adopt the scale-discretised wavelet transform on the sphere (Wiaux, McEwen *et al.* 2008), where we denote the wavelet coefficients of the data d by $\boxed{W^d_{j\rho} = \langle d,\ \Psi_{j\rho} \rangle}$ for scale $j \in \mathbb{Z}^+$ and position $\rho \in \mathrm{SO}(3)$.
- Consider an even azimuthal band-limit $N = 4$ to yield wavelet with odd azimuthal symmetry.

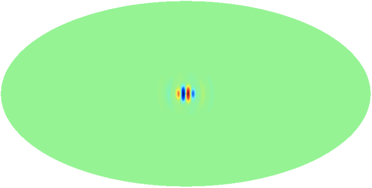

Figure: Example wavelet.

- Wavelet transform yields a sparse representation of the string signal $\rightarrow$ hope to effectively separate the CMB and string signal in wavelet space.

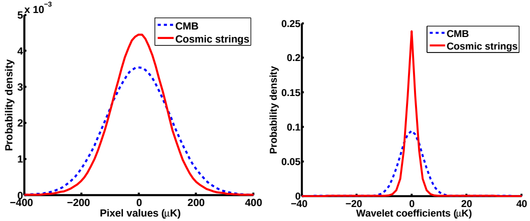

Figure: Distribution of CMB and string signal in pixel (left) and wavelet space (right).

Learning the statistics of the CMB and string signals in wavelet space

- Need to determine statistical description of the CMB and string signals in wavelet space.
- Calculate analytically the probability distribution of the CMB in wavelet space:

$$\mathrm{P}_j^c(W_{j\rho}^c) = \frac{1}{\sqrt{2\pi(\sigma_j^c)^2}} \mathrm{e}^{\left(-\frac{1}{2}\left(\frac{W_{j\rho}^c}{\sigma_j^c}\right)^2\right)}, \quad \text{where} \quad (\sigma_j^c)^2 = \langle W_{j\rho}^c \, W_{j\rho}^{c\;*} \rangle = \sum_{\ell m} C_\ell \, |(\Psi_j)_{\ell m}|^2 \, .$$

- Fit a generalised Gaussian distribution (GGD) for the wavelet coefficients of a string training map (*cf.* Wiaux *et al.* 2009):

$$\mathrm{P}_j^s(W_{j\rho}^s \mid G\mu) = \frac{\upsilon_j}{2G\mu\nu_j\Gamma(\upsilon_j^{-1})} \mathrm{e}^{\left(-\left|\frac{W_{j\rho}^s}{G\mu\nu_j}\right|^{\upsilon_j}\right)},$$

with scale parameter ν_j and shape parameter υ_j.

Learning the statistics of the CMB and string signals in wavelet space

- Need to determine statistical description of the CMB and string signals in wavelet space.
- Calculate analytically the probability distribution of the CMB in wavelet space:

$$\mathrm{P}_j^c(W_{j\rho}^c) = \frac{1}{\sqrt{2\pi(\sigma_j^c)^2}} \, \mathrm{e}^{\left(-\frac{1}{2}\left(\frac{W_{j\rho}^c}{\sigma_j^c}\right)^2\right)} \, , \quad \text{where} \quad (\sigma_j^c)^2 = \langle W_{j\rho}^c \, W_{j\rho}^{c\;*} \rangle = \sum_{\ell m} C_\ell \, |(\Psi_j)_{\ell m}|^2 \, .$$

- Fit a generalised Gaussian distribution (GGD) for the wavelet coefficients of a string training map (*cf.* Wiaux *et al.* 2009):

$$\mathrm{P}_j^s(W_{j\rho}^s \mid G\mu) = \frac{\upsilon_j}{2G\mu\nu_j\Gamma(\upsilon_j^{-1})} \, \mathrm{e}^{\left(-\left|\frac{W_{j\rho}^s}{G\mu\nu_j}\right|^{\upsilon_j}\right)} \, ,$$

with scale parameter ν_j and shape parameter υ_j.

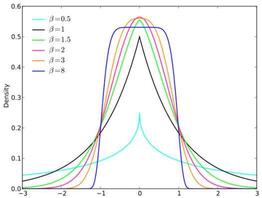

Figure: Generalised Gaussian distribution (GGD).

Learning the statistics of the CMB and string signals in wavelet space

- Require two simulated string maps: one for training; one for testing.

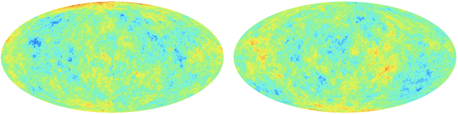

(a) String1 (b) String2

Figure: Cosmic string simulations.

- Compare distribution learnt from the training simulation (string2) with the distribution of the testing simulation (string1).
- Distributions in close agreement.

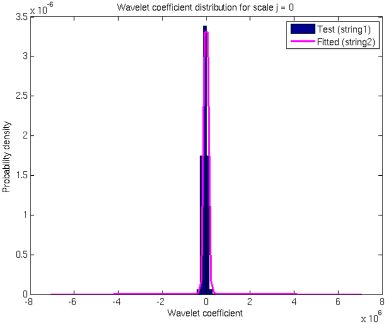

Figure: Distributions for wavelet scale $j = 0$.

Learning the statistics of the CMB and string signals in wavelet space

- Require two simulated string maps: one for training; one for testing.

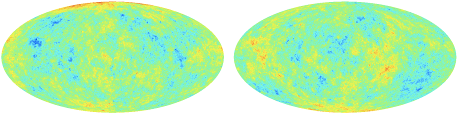

(a) String1 (b) String2

Figure: Cosmic string simulations.

- Compare distribution learnt from the training simulation (string2) with the distribution of the testing simulation (string1).
- Distributions in close agreement.

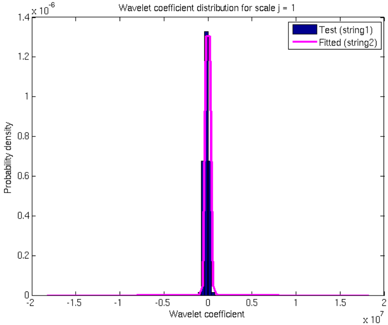

Figure: Distributions for wavelet scale $j = 1$.

Learning the statistics of the CMB and string signals in wavelet space

- Require two simulated string maps: one for training; one for testing.

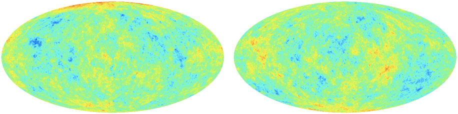

(a) String1 (b) String2

Figure: Cosmic string simulations.

- Compare distribution learnt from the training simulation (string2) with the distribution of the testing simulation (string1).
- Distributions in close agreement.

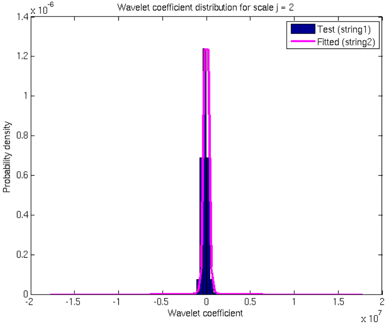

Figure: Distributions for wavelet scale $j = 2$.

Learning the statistics of the CMB and string signals in wavelet space

- Require two simulated string maps: one for training; one for testing.

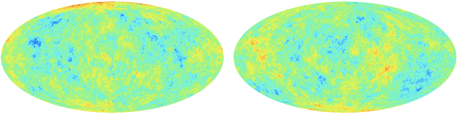

(a) String1 (b) String2

Figure: Cosmic string simulations.

- Compare distribution learnt from the training simulation (string2) with the distribution of the testing simulation (string1).
- Distributions in close agreement.

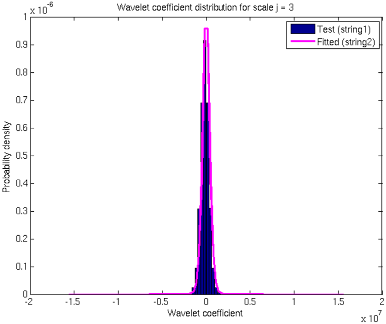

Figure: Distributions for wavelet scale $j = 3$.

Learning the statistics of the CMB and string signals in wavelet space

- Require two simulated string maps: one for training; one for testing.

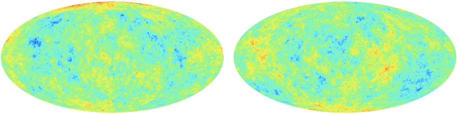

(a) String1 (b) String2

Figure: Cosmic string simulations.

- Compare distribution learnt from the training simulation (string2) with the distribution of the testing simulation (string1).
- Distributions in close agreement.

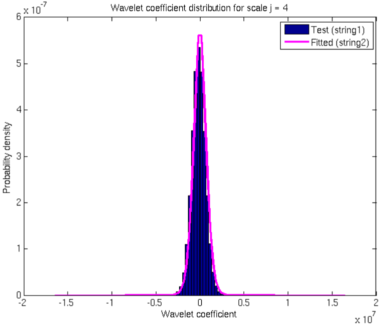

Figure: Distributions for wavelet scale $j = 4$.

Learning the statistics of the CMB and string signals in wavelet space

- Require two simulated string maps: one for training; one for testing.

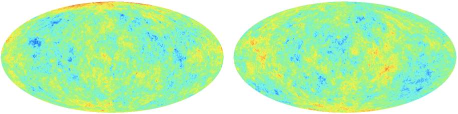

(a) String1 (b) String2

Figure: Cosmic string simulations.

- Compare distribution learnt from the training simulation (string2) with the distribution of the testing simulation (string1).
- Distributions in close agreement.
- We have accurately characterised the statistics of string signals in wavelet space.

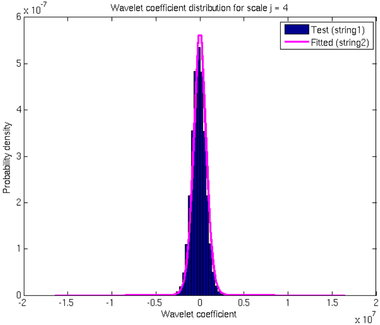

Figure: Distributions for wavelet scale $j = 4$.

Spherical wavelet-Bayesian string tension estimation

- Perform Bayesian string tension estimation in wavelet space, where the CMB and string distributions are very different.

- For each wavelet coefficient the likelihood is given by

$$P(W^d_{j\rho} \mid G\mu) = P(W^s_{j\rho} + W^c_{j\rho} \mid G\mu) = \int_{\mathbb{R}} dW^s_{j\rho}\, P^c_j(W^d_{j\rho} - W^s_{j\rho})\, P^s_j(W^s_{j\rho} \mid G\mu) \, .$$

- The overall likelihood of the data is given by

$$P(W^d \mid G\mu) = \prod_{j,\rho} P(W^d_{j\rho} \mid G\mu) \, ,$$

where we have assumed independence.

Spherical wavelet-Bayesian string tension estimation

- Perform Bayesian string tension estimation in wavelet space, where the CMB and string distributions are very different.
- For each wavelet coefficient the likelihood is given by

$$\mathrm{P}(W^d_{j\rho} \mid G\mu) = \mathrm{P}(W^s_{j\rho} + W^c_{j\rho} \mid G\mu) = \int_{\mathbb{R}} \mathrm{d}W^s_{j\rho} \, \mathrm{P}^c_j(W^d_{j\rho} - W^s_{j\rho}) \, \mathrm{P}^s_j(W^s_{j\rho} \mid G\mu) \, .$$

- The overall likelihood of the data is given by

$$\mathrm{P}(W^d \mid G\mu) = \prod_{j,\rho} \mathrm{P}(W^d_{j\rho} \mid G\mu) \, ,$$

where we have assumed independence.

Spherical wavelet-Bayesian string tension estimation

- Compute the string tension posterior $\text{P}(G\mu \mid W^d)$ by Bayes theorem:

$$\text{P}(G\mu \mid W^d) = \frac{\text{P}(W^d \mid G\mu)\,\text{P}(G\mu)}{\text{P}(W^d)} \propto \text{P}(W^d \mid G\mu)\,\text{P}(G\mu)\,.$$

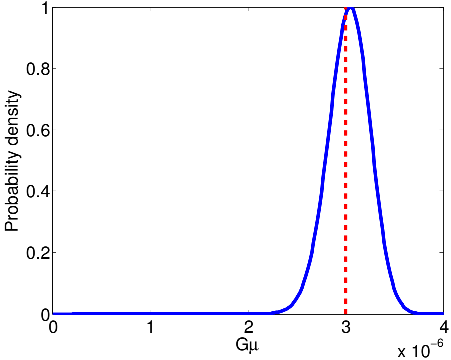

Figure: Posterior distribution of the string tension (true $G\mu = 3 \times 10^{-6}$).

Spherical wavelet-Bayesian string tension estimation

- Compute the string tension posterior $\mathrm{P}(G\mu \mid W^d)$ by Bayes theorem:

$$\mathrm{P}(G\mu \mid W^d) = \frac{\mathrm{P}(W^d \mid G\mu)\,\mathrm{P}(G\mu)}{\mathrm{P}(W^d)} \propto \mathrm{P}(W^d \mid G\mu)\,\mathrm{P}(G\mu)\ .$$

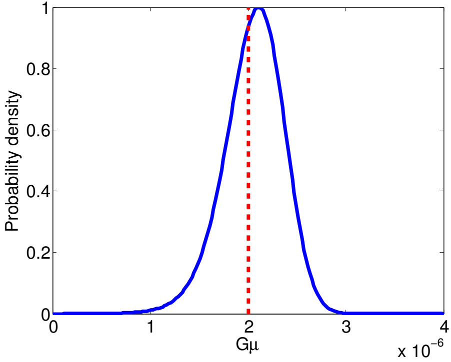

Figure: Posterior distribution of the string tension (true $G\mu = 2 \times 10^{-6}$).

Spherical wavelet-Bayesian string tension estimation

- Compute the string tension posterior $\mathrm{P}(G\mu \mid W^d)$ by Bayes theorem:

$$\mathrm{P}(G\mu \mid W^d) = \frac{\mathrm{P}(W^d \mid G\mu)\, \mathrm{P}(G\mu)}{\mathrm{P}(W^d)} \propto \mathrm{P}(W^d \mid G\mu)\, \mathrm{P}(G\mu)\ .$$

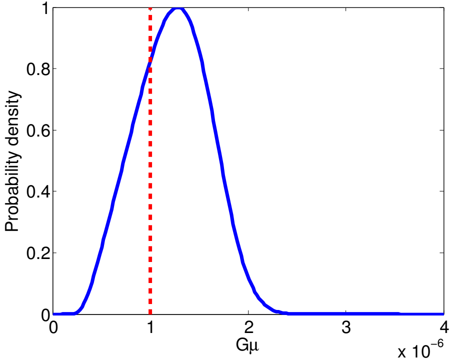

Figure: Posterior distribution of the string tension (true $G\mu = 1 \times 10^{-6}$).

Bayesian evidence for strings

- Compute Bayesian evidences to compare the string model M^s to the alternative model M^c that the observed data is comprised of just a CMB contribution.

- The Bayesian evidence of the string model is given by

$$E^s = \mathrm{P}(W^d \mid \mathrm{M}^s) = \int_{\mathbb{R}} \mathrm{d}(G\mu)\, \mathrm{P}(W^d \mid G\mu)\, \mathrm{P}(G\mu) \ .$$

- The Bayesian evidence of the CMB model is given by

$$E^c = \mathrm{P}(W^d \mid \mathrm{M}^c) = \prod_{j,\rho} \mathrm{P}^c_j(W^d_{j\rho}) \ .$$

- Compute the Bayes factor to determine the preferred model:

$$\Delta \ln E = \ln(E^s / E^c) \ .$$

Table: Tension estimates and log-evidence differences for simulations.

$G\mu/10^{-6}$	0.7	0.8	0.9	1.0	2.0	3.0
$\widehat{G\mu}/10^{-6}$	1.1	1.2	1.2	1.3	2.1	3.1
$\Delta \ln E$	-1.3	-1.1	-0.9	-0.7	5.5	29

Recovering string maps

- Our best inference of the wavelet coefficients of the underlying string map is encoded in the posterior probability distribution $\mathrm{P}(W^s_{j\rho} \mid W^d)$.

- Estimate the wavelet coefficients of the string map from the mean of the posterior distribution:

$$\overline{W}^s_{j\rho} = \int_{\mathbb{R}} \mathrm{d}W^s_{j\rho}\; W^s_{j\rho}\; \mathrm{P}(W^s_{j\rho} \mid W^d)$$
$$= \int_{\mathbb{R}} \mathrm{d}(G\mu)\; \mathrm{P}(G\mu \mid d)\; \overline{W}^s_{j\rho}(G\mu)\ ,$$

where

$$\overline{W}^s_{j\rho}(G\mu) = \int_{\mathbb{R}} \mathrm{d}W^s_{j\rho}\; W^s_{j\rho}\; \mathrm{P}(W^s_{j\rho} \mid W^d_{j\rho}, G\mu)$$
$$= \frac{1}{\mathrm{P}(W^d_{j\rho} \mid G\mu)} \int_{\mathbb{R}} \mathrm{d}W^s_{j\rho}\; W^s_{j\rho}\; \mathrm{P}^c_j(W^d_{j\rho} - W^s_{j\rho})\; \mathrm{P}^s_j(W^s_{j\rho} \mid G\mu)\ .$$

- Recover the string map from its wavelets (possible since the scale-discretised wavelet transform on the sphere supports exact reconstruction).

- Work in progress. . .

Summary

- Observations on spherical manifolds are prevalent.
- Necessitate rigorous signal processing techniques on spherical manifolds:
  - Sampling theorems
  - Wavelets
  - Compressive sensing
- In cosmology, sensitive methods are required to extract the weak signatures of new physics from next-generation observations.

Extra slides on compressive sensing

Introduction to the theory of compressive sensing

- Linear operator (linear algebra) representation of wavelet decomposition:

$$x(t) = \sum_i \alpha_i \Psi_i(t) \quad \rightarrow \quad \boldsymbol{x} = \sum_i \Psi_i \alpha_i = \begin{pmatrix} | \\ \Psi_0 \\ | \end{pmatrix} \alpha_0 + \begin{pmatrix} | \\ \Psi_1 \\ | \end{pmatrix} \alpha_1 + \cdots \quad \rightarrow \quad \boldsymbol{x} = \Psi \boldsymbol{\alpha}$$

- Linear operator (linear algebra) representation of measurement:

$$y_i = \langle x, \Phi_j \rangle \quad \rightarrow \quad \boldsymbol{y} = \begin{pmatrix} - & \Phi_0 & - \\ - & \Phi_1 & - \\ & \vdots & \end{pmatrix} \boldsymbol{x} \quad \rightarrow \quad \boldsymbol{y} = \Phi \boldsymbol{x}$$

- Putting it together: $\boldsymbol{y} = \Phi \boldsymbol{x} = \Phi \Psi \boldsymbol{\alpha}$

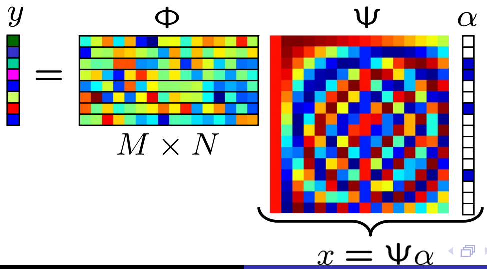

Introduction to the theory of compressive sensing

- In the absence of noise, compressed sensing is **exact!**
- Number of measurements required to achieve exact reconstruction is given by

$$M \geq c\mu^2 K \log N \ ,$$

where K is the sparsity and N the dimensionality.

- The coherence between the measurement and sparsity basis is given by

$$\mu = \sqrt{N} \max_{i,j} |\langle \Psi_i, \Phi_j \rangle| \ .$$

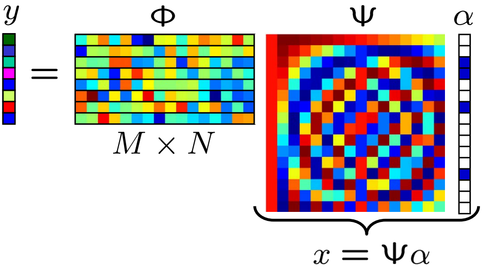

- Robust to noise.
- Many new developments (*e.g.* analysis vs synthesis, cosparsity, structured sparsity) and new applications.

Extra slides on sparsity averaging

SARA for radio interferometric imaging

- Sparsity averaging reweighted analysis (SARA) algorithm (Carrillo, McEwen & Wiaux 2012)
- Consider a dictionary composed of a concatenation of orthonormal bases, i.e.

$$\Psi = \frac{1}{\sqrt{q}}[\Psi_1, \Psi_2, \ldots, \Psi_q],$$

thus $\Psi \in \mathbb{R}^{N\times D}$ with $D = qN$.

- We consider the following bases:
  - Dirac, *i.e.* pixel basis
  - Haar wavelets (promotes gradient sparsity)
  - Daubechies wavelet bases two to eight.

$\Rightarrow$ concatenation of 9 bases

- Promote average sparsity by solving the reweighted ℓ_1 analysis problem:

$$\min_{\bar{\boldsymbol{x}}\in\mathbb{R}^N} \|W\Psi^T\bar{\boldsymbol{x}}\|_1 \quad \text{subject to} \quad \|\boldsymbol{y}-\Phi\bar{\boldsymbol{x}}\|_2 \leq \epsilon \quad \text{and} \quad \bar{\boldsymbol{x}} \geq 0\,,$$

where $W \in \mathbb{R}^{D\times D}$ is a diagonal matrix with positive weights.

- Solve a sequence of reweighted ℓ_1 problems using the solution of the previous problem as the inverse weights $\rightarrow$ approximate the ℓ_0 problem.

SARA for radio interferometric imaging

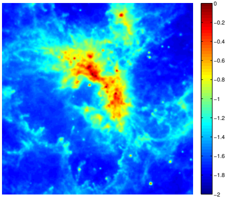

(a) Original

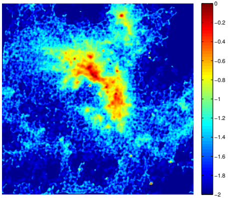

(b) BP (SNR=16.67 dB)

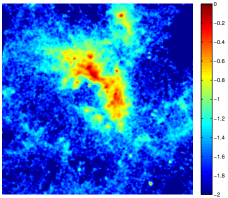

(c) IUWT (SNR=17.87 dB)

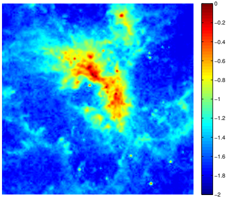

(d) BPDb8 (SNR=24.53 dB)

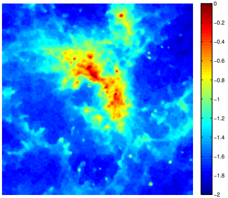

(e) TV (SNR=26.47 dB)

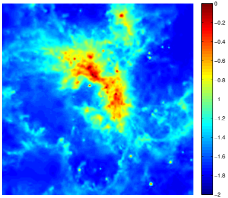

(f) SARA (SNR=29.08 dB)

Figure: Reconstruction example of 30Dor from 30% of visibilities.